

# Assessing distances and consistency of kinematics in Gaia/TGAS

Ralph Schönrich<sup>★</sup> and Michael Aumer

*Rudolf Peierls Centre for Theoretical Physics, 1 Keble Road, Oxford, OX1 3NP, UK*

Draft, 24 November 2018

## ABSTRACT

We apply the statistical methods by Schönrich, Binney & Asplund to assess the quality of distances and kinematics in the RAVE-TGAS and LAMOST-TGAS samples of Solar neighbourhood stars. These methods yield a nominal distance accuracy of 1–2%. Other than common tests on parallax accuracy, they directly test distance estimations including the effects of distance priors. We show how to construct these priors including the survey selection functions (SSFs) directly from the data. We demonstrate that neglecting the SSFs causes severe distance biases. Due to the decline of the SSFs in distance, the simple 1/parallax estimate only mildly underestimates distances. We test the accuracy of measured line-of-sight velocities ( $v_{\text{los}}$ ) by binning the samples in the nominal  $v_{\text{los}}$  uncertainties. We find: a) the LAMOST  $v_{\text{los}}$  are generally underestimated by  $\sim 5 \text{ km s}^{-1}$ ; b) the average LAMOST measurement error for  $v_{\text{los}}$  is  $\sim 7 \text{ km s}^{-1}$ , significantly smaller than, and nearly uncorrelated with the nominal LAMOST estimates. The RAVE sample shows either a moderate distance underestimate, or an unaccounted source of  $v_{\text{los}}$  dispersion ( $e_{\parallel}$ ) from measurement errors and binary stars. For a subsample of suspected binary stars in RAVE, our methods indicate significant distance underestimates. Separating a sample in metallicity or kinematics to select thick-disc/halo stars, discriminates between distance bias and  $e_{\parallel}$ . For LAMOST, this separation yields consistency with pure  $v_{\text{los}}$  measurement errors. We find an anomaly near longitude  $l \sim (300 \pm 60)^{\circ}$  and distance  $s \sim (0.32 \pm 0.03) \text{ kpc}$  on both sides of the galactic plane, which could be explained by either a localised distance error or a breathing mode.

**Key words:** stellar parallaxes – stars: distances – stars: kinematics and dynamics – Galaxy: kinematics and dynamics – Galaxy: solar neighbourhood

## 1 INTRODUCTION

The Gaia satellite mission (Perryman et al. 1997) is the most important survey of this decade for the fields of Galactic and stellar astronomy. It is retrieving precision astrometry for of order one billion stars throughout the Galaxy, coupled to spectroscopic observations that allow determination of stellar parameters and line-of-sight velocities for a large subset of these stars. In addition, this effort is coupled to a plethora of ground-based spectroscopic surveys, including RAVE, Gaia-ESO, APOGEE, SEGUE, GALAH, LAMOST, and WEAVE.

Since the first release of Tycho-Gaia Astrometric Solution (TGAS) data (Gaia Collaboration 2016; Lindegren et al. 2016) there has been a variety of papers examining the quality of the data, ranging from the original validation paper (Lindegren et al. 2016) to studies with

standard candles, like red giants and red giant clump stars (de Ridder et al. 2016; Davies et al. 2017). A thorough compilation of standard validations of TGAS astrometry is found in Arenou et al. (2017). They discuss significant deviations of the median parallax from 0 for remote objects in different regions of the sky, e.g. for objects in the Magellanic Clouds. Most such quality tests for parallaxes  $p$  rely on distant objects, which should have  $p = 0$ , i.e. quasars, galaxies, or objects in neighbouring galaxies. For such tests the main caveats are potential contamination with Galactic sources, and to a minor extent their different geometry, and different spectral distribution.

For Milky Way studies, it is vital to have a direct validation also of larger parallax measurements. However, well-constrained standard candles like Cepheids are not numerous enough to allow for resolved, high-precision testing. Most other types of standard candles, like RR Lyrae stars, Red Clump stars, or Blue Horizontal Branch stars are more distant than the local dwarf star samples. More importantly,

<sup>★</sup> E-mail: ralph.schoenrich@physics.ox.ac.uk



## 2 DATA AND DEFINITIONS

### 2.1 Coordinate frame and definitions

For all subsequent discussions, please refer to Fig. 2 for definitions of our coordinate frame. We discriminate between the heliocentric cartesian frame where the velocities are termed  $(U, V, W)$  radially towards the Galactic centre, azimuthally in the direction of Galactic rotation, and vertically out of the plane. We also use velocities in the galactocentric cylindrical coordinate frame, marked by indices  $g$ , naming the velocity vector  $(U_g, V_g, W)$ ; the vertical direction is fixed. The galactocentric radius is termed  $R$ , the distance to the Galactic Centre  $r$ . The angle  $\beta = \tan^{-1}(z/R)$  is the angle between the Galactic plane and the connection line star-Galactic centre. The angle between the Sun-centre and the star-centre connection lines is called  $\alpha$ . Galactic longitude and latitude are termed  $l$  and  $b$ . The Sun's galactocentric distance  $R_0 = 8.27$  kpc, azimuthal velocity  $v_\odot = 248$  km s<sup>-1</sup>, and motion with respect to the LSR  $(U_\odot, V_\odot, W_\odot) = (13, 12.24, 7.24)$  km s<sup>-1</sup> are chosen in concordance with Schönrich (2012), McMillan (2011), and Schönrich et al. (2010).

### 2.2 TGAS data

For this work, we crossmatch TGAS data from Gaia DR1 (Gaia Collaboration 2016; Lindegren et al. 2016) both with RAVE DR5 (Kunder et al. 2016) and with DR2 of LAMOST (Luo et al. 2015). As can be seen in Fig. 1, the samples would together provide a full sky coverage. While LAMOST DR2 has far more stars, the catalogue covers significantly fainter stars giving a smaller common footprint with TGAS. More importantly, LAMOST's line-of-sight velocity determinations are about one order of magnitude less precise than in the RAVE survey, so on LAMOST our statistics will rather test their  $v_{\text{los}}$  measurements than the distances. To ensure sufficient quality of the data, we adopt a few general cuts:

- A derived distance  $s > 30$  pc. Lindegren et al. (2016) report that TGAS is biased against stars with a proper motion larger than  $3.5''$  yr<sup>-1</sup>. To prevent kinematic bias (a cut in proper motions might feign a distance underestimate) we drop all stars with  $s < 30$  pc, where the proper motion cut would translate into a transverse velocity relative to the Sun  $|v_\perp| > 500$  km s<sup>-1</sup>. This affects only a handful of stars.
- Limiting  $-100 < V_g/\text{km s}^{-1} < 310$ : again this cut in heliocentric azimuthal velocity affects only a handful of stars, and we have tested that our results are robust against the precise choice. However, damaged data tend to assemble in the extreme wings, so it is a cleaner decision to drop them.
- Limiting the line-of-sight motion  $|v_{\text{los}}| < 500$  km s<sup>-1</sup>: this cut also affects only a handful of objects. However, in particular in RAVE we have indication that a few erroneous velocity determinations assemble at the extreme values.

### 2.3 RAVE

The RAVE DR5 sample contains 520 701 entries. However, about 15% of the entries are multiple measurements of the same object. Of the 68 822 duplicate entries, we choose the one that has a smaller radial velocity (RV) error given by the RAVE pipeline, leaving us with 451 879 unique stars. To test the crossmatch between the RAVE DR5 sample with

TGAS, we have compared two different strategies: a) using the already crossmatched positions in Kunder et al. (2016) and demanding a precise match in position to the Gaia catalogues, which gives us 210 415 crossmatched stars, and b) using the positions in RAVE vs. TGAS positions and proper motions, demanding that the position and proper motion in TGAS predicts within 3 arcseconds the original position in the RAVE catalogue. The latter exercise gives us 215 640 stars. We note here that to calculate the latter properly, we needed to use the year 2000 equinox: while the Gaia data are given at the Gaia epoch of 2015.0, they use the 2000.0 equinox, i.e. orientation of Earth and the RA-DEC system at that time. We have compared our results from the different selections and crossmatches, and since these choices do not significantly affect our results, we report here only results for the original RAVE DR5 crossmatch. We further exclude all stars that are flagged as cluster members in the RAVE dataset, or have a line-of-sight velocity error given as  $\sigma_{\text{los,RAVE}} = 0$  km s<sup>-1</sup>. If not explicitly stated otherwise, we use the quality cut  $\sigma_{\text{los,RAVE}} < 5$  km s<sup>-1</sup>, which will be justified in Section 5.2. A large number of stars in this cross-matched sample will fail our variable cut for the precision of the measured TGAS parallax. E.g. the RAVE subsample under our quality restrictions with parallaxes ( $p_0$ ) better than 20%, i.e.  $p_0/\sigma_p > 5$ , has only 88 516 members.

An important classification of RAVE spectra is given by the flags from Matijević et al. (2012). These flags list the 20 closest matches to each RAVE spectrum for different classes of stars, e.g. normal stars (marked with 'n'), chromospherically active stars, or suspected binaries. Throughout this paper we use these flags to define three subsets of RAVE: a) all stars in RAVE irrespective of their classification, b) unflagged stars, i.e. stars that have all 20 flags set to 'n', and c) suspected binaries, which have at least one flag set to 'b'.

### 2.4 LAMOST

To crossmatch the LAMOST sample with TGAS, we use the TGAS proper motions and positions to calculate back to the suspected position in LAMOST at epoch 2000. For a proper match we demand  $\sqrt{\Delta_{\text{RA}}^2 + \Delta_{\text{DEC}}^2} < 1.2 \times 10^{-3}$  deg (or equivalently  $< 4.3''$ ), between the predicted position and the position given in the LAMOST catalogue. Repeat observations in LAMOST are purged by taking for each object in TGAS the best match in position, or at equal match, the latest entry in the LAMOST catalogue. This leaves us with 107 663 stars in the crossmatched sample. To avoid kinematic biases in the selection function, which could affect our statistics, we remove the region of  $0 < \text{RA deg}^{-1} < 67$  and  $42 < \text{DEC deg}^{-1} < 59$  from the LAMOST sample, since Luo et al. (2015) report that this region contains a subsample of plates that have a proper motion selection, limiting the stellar proper motions to smaller than  $7$  mas yr<sup>-1</sup>. There might be minor contamination of in-plane fields with kinematic selections, but since the distance statistics we choose for this analysis are not sensitive to stars in the Galactic Plane, we judge the above exclusion region to be safe. Demanding a parallax uncertainty better than 20% and a signal to noise ratio  $\text{SNR} > 30$ , the usual line-of-sight velocity cut  $|v_{\text{los}}| < 500$  km s<sup>-1</sup> and a galactocentric azimuthal velocity of  $-100 < V_g/\text{km s}^{-1} < 310$ , we have a remaining sample

of 34 384 stars. The signal to noise cut is not overly important, since the cross-match with Gaia includes mostly bright objects; with a cut at  $\text{SNR} > 5$  we would have 38 834 stars.

We will show in Section 5.2 that line-of-sight velocities in LAMOST have to be corrected by adding  $\delta v_{\text{los}} = 5 \text{ km s}^{-1}$ . Further, we will limit the sample to a nominal  $v_{\text{los}}$  measurement error  $\sigma_{\text{los,LAM}} < 27 \text{ km s}^{-1}$ , and replace their estimate by using  $\sigma_{\text{los}} = 7.2 \text{ km s}^{-1}$ , motivated by Section 5.5.

### 3 DISTANCE DETERMINATIONS

For the sake of well-defined error distributions in our distance determination, we will rely solely on parallaxes. Since the reported parallax errors are all larger than  $0.2 \text{ mas}$ , a 10% (or 20%) quality cut on the parallax will limit the sample to within  $\sim 0.5 \text{ kpc}$  (1 kpc), with some weak dependence on the used prior. With parallax errors still a significant fraction of the measured parallax, it is not advisable to just use the inverse parallax as a distance. For the derivation of distances from parallaxes, see Strömberg (1927), Schönrich & Bergemann (2014), or Astraatmadja & Bailer-Jones (2016). Since we are using exclusively the parallaxes to assess stellar distances, the magnitude based selection function of the sample has to be written into the prior, so that our estimator for the distance of each star is:

$$\langle s \rangle = N^{-1} \int ds s^3 G(p, p_0, \sigma_p) \rho(s(p), l, b) S(s(p)), \quad (1)$$

where

$$N = \int ds s^2 G(p, p_0, \sigma_p) \rho(s(p), l, b) S(s(p)) \quad (2)$$

is the normalisation.  $G(p, p_0, \sigma_p)$  is the observational likelihood of the parallax given the measurement  $(p_0, \sigma_p)$ ,  $s^2$  is the geometric factor, i.e. surface of the observational cone at fixed distance  $s$ ,  $\rho(s, l, b)$  is the supposed density of stars in direction of galactic longitude and latitude  $(l, b)$ , and  $S$  is the selection function, which we approximate as a function of distance  $s$  only. For the density prior  $\rho$ , we use the simple thin/thick disc + halo decomposition from equation (32) in Schönrich & Bergemann (2014), i.e. our density model simply reads as:

$$\rho(R, z) = e^{-\frac{(R-R_0)}{R_d}} e^{-\frac{|z|}{z_0}} + a_t e^{-\frac{(R-R_0)}{R_d}} e^{-\frac{|z|}{z_{0,t}}} + a_h \left(\frac{r}{R_0}\right)^{-2.5}, \quad (3)$$

where  $R$  is the galactocentric radius in cylindrical coordinates,  $R_0$  is the (cylindrical) galactocentric radius of the Sun,  $R_d$  is the scale-length of the disc, chosen at  $R_d = 2.5 \text{ kpc}$ ,  $z$  the altitude above the plane,  $z_0 = 0.3 \text{ kpc}$  and  $z_{0,t} = 0.9 \text{ kpc}$  are the scale-heights of the thin and thick disc,  $r$  is the galactic centre distance used for a simple spherical halo model,  $a_t = 0.12$  is a local thick disc normalisation set in concordance with Ivezić et al. (2008),  $a_h = 0.001$  normalises the halo component. For this calculation, we neglect the small offset of the Sun from the galactic plane.

The selection function  $S$  would typically require the use of a full population synthesis model: It is apparent that the magnitude limits of the RAVE survey will introduce a strong bias towards more nearby stars and for brighter objects, which ultimately favours younger stellar populations. Stellar metallicities affect their brightness and colour, thus affecting

the selection function as well. While  $S$  will hence in general not be spatially uniform, we approximate  $S(s)$  as a function of distance  $s$  only. We discuss its derivation in Section 5.3.1.

### 4 ASSESSING DISTANCES AND LINE-OF-SIGHT VELOCITY DISTRIBUTION ERRORS

To assess distances we make use of the statistical distance method of SBA, where also a full derivation of all equations can be found. In addition to the theoretical justification, we have performed numerous validations on the original method. Since we are using a restricted approach in this paper, we present in the Appendix a short validation on N-body galaxy simulations, which are structurally similar to the Milky Way.

This method exploits position dependent correlations between different heliocentric velocity components, using the fact that systematic distance errors lead to a mixing term between velocities. A stellar motion relative to the Sun  $(U_0, V_0, W_0)$  results in observable line-of-sight velocity  $v_{\text{los}}$  and proper motions  $\mu_l$  and  $\mu_b$ , depending on the distance  $s_0$  to the star, calculated with the translation matrix  $\mathbf{M}$ . Since this translation matrix is orthogonal, we have

$$\begin{pmatrix} U_0 \\ V_0 \\ W_0 \end{pmatrix} = \mathbf{M} \begin{pmatrix} s\mu_l \\ s\mu_b \\ v_{\text{los}} \end{pmatrix} \quad \text{and} \quad \begin{pmatrix} s\mu_l \\ s\mu_b \\ v_{\text{los}} \end{pmatrix} = \mathbf{M}^T \begin{pmatrix} U_0 \\ V_0 \\ W_0 \end{pmatrix} \quad (4)$$

If our distance estimate  $s$  for the star is wrong by a fraction  $f$ , the terms containing the proper motions will be stretched by  $(1+f) = s/s_0$ , and our estimated velocity vector  $(U, V, W)$  for the star will be altered to

$$\begin{pmatrix} U \\ V \\ W \end{pmatrix} = (\mathbf{I} + f\mathbf{T}) \begin{pmatrix} U_0 \\ V_0 \\ W_0 \end{pmatrix}, \quad (5)$$

where  $\mathbf{T} = \mathbf{M}\mathbf{P}\mathbf{M}^T$ ,  $\mathbf{I}$  is the identity matrix, and  $\mathbf{P}$  is the identity for the proper motion terms, but zero in the  $v_{\text{los}}$  term. For the following discussion, we only need the terms of  $\mathbf{T}$  connecting the vertical motion to all velocity components, i.e.

$$\begin{aligned} T_{UW} &= \cos(l) \sin(b) \cos(b), \\ T_{VW} &= \sin(l) \sin(b) \cos(b), \quad \text{and} \\ T_{WW} &= \cos^2(b). \end{aligned} \quad (6)$$

Take for example the motion of the Sun against a sample of halo stars. The Sun has an azimuthal velocity of roughly  $V_0 \sim 250 \text{ km s}^{-1}$ , while halo stars have no net azimuthal motion.  $T_{VW}$  is maximal when we look up out of the galactic plane at an angle  $b \sim 45^\circ$  in or against the direction of solar motion. To get a picture on how this term links vertical heliocentric velocities  $W$  with azimuthal velocities  $V$ , imagine approaching horizontally the wall of your room, while looking at the corners of the floor and the ceiling. Both corners will be blue-shifted in their line-of sight velocity, but you also observe an angular motion. If your distance estimate to the corners is correct, the conclusion will be a zero net motion of the room. However, if the distance is over-estimated, the angular motion of the upper corner will be mistakenly translated into a net upwards motion, and similarly, the lower corner will appear to move downwards. Similarly, if we

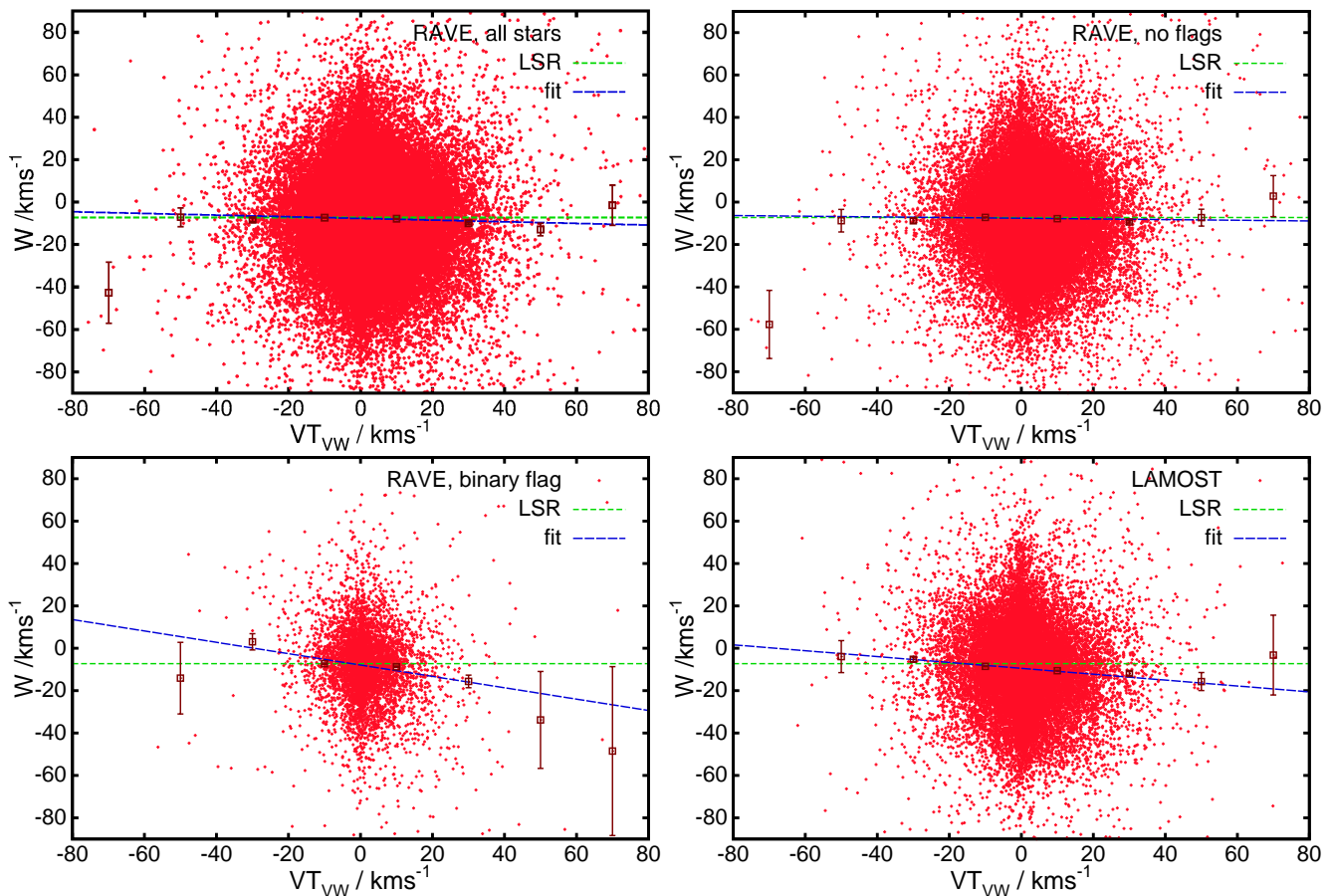


**Figure 3.** Trends in  $W$  vs.  $VT_{VW}$  in all RAVE stars (top left), all unflagged RAVE stars with at least one binary flag (bottom left), and all LAMOST stars with  $\sigma_{\text{los,LAM}} < 25 \text{ km s}^{-1}$  (bottom right). The dark red errorbars show the mean values of  $W$  when binning the sample along the x-axis. The green short dashed line marks the reflex motion of the Sun, the blue long-dashed line the linear fit to the data. Despite the curious outliers at extreme azimuthal velocities in the RAVE sample, the slopes in all four plots are significant and given in Table 1.

overestimate stellar distances in our Galactic halo example, we will detect a net upwards motion (positive  $W$ ) maximal near  $(l, b) \sim (90^\circ, 45^\circ)$ , and  $(l, b) \sim (270^\circ, -45^\circ)$  and a downwards motion (negative  $W$ ) around  $(l, b) \sim (90^\circ, -45^\circ)$ , and  $(l, b) \sim (270^\circ, 45^\circ)$ , and opposite bias for a distance underestimate. This motion will be proportional to the azimuthal velocity difference between the Sun and the stars.

As discussed in SBA, there are similar connections between each velocity pair. However, since we are dealing with a disc sample with a complicated selection function and strive for maximum accuracy, we will drop all terms that are to first order affected by galactic rotation and streaming ( $U$  vs.  $V$  motion). Since proper motion errors are minimal, we can use the more precise non-linear estimator from SBA.

As a quick test for distance errors in a sample of stars, we can assume that  $(U, V, W)$  is sufficiently close to the real velocity vector  $(U_0, V_0, W_0)$  and fit a straight line to  $W$  vs.  $T_{VW}V$ , via the regression model

$$W_i = \gamma T_{VW,i} V_i - W_\odot + \epsilon_i, \quad (7)$$

where  $W_i$  and  $V_i$  are the measured vertical and azimuthal velocity components for the  $i$ th star, and  $T_{VW,i}$  is given in equation (6). The fit parameters  $W_\odot$  and  $\gamma$ , represent the vertical motion of the Sun, and the average fractional distance error,  $\epsilon_i$  represents the random term from stellar veloc-

ity dispersion and measurement errors. These fits are shown in Fig. 3 for different subsamples of RAVE-TGAS, and for LAMOST-TGAS. The dark red errorbars show means of  $W$  when binning the sample in  $VT_{VW}$ , while the blue dashed lines show the fitted regression line from equation (7). It is evident that in particular LAMOST and the suspected binary stars in RAVE show a large slope  $\gamma$ , indicating either a major distance bias, or a problem with line-of-sight velocity determination.

We note that a robust linear estimator can be derived from equation (7) by replacing the individual azimuthal velocities with their expectation value, i.e.  $V_i \rightarrow \langle V \rangle$ . This estimator is particularly useful for remote samples of halo stars with a large mean heliocentric  $V$ . However, for disc stars this estimator is about one order of magnitude less sensitive than our full estimator, and so for this work of little use compared to the full distance estimator, which we will now describe.

The regression in equation (7) can be formalised to an estimate of the fractional distance error  $f_{UV}$ . We adopt equation (19) from SBA:

$$f = \frac{\text{Cov}(W, y)}{\text{Var}(y) + \langle (T_{VW}^2 + T_{UW}^2) \sigma_W^2 \rangle}, \quad (8)$$

where  $y = T_{UW}U + T_{VW}V - T_{WV}W_\odot$  is the “baseline” on which

the rise in  $W$  is measured,  $\text{Cov}$  is the covariance, and  $\text{Var}(y)$  is the variance of  $y$ . To measure the distance bias in practice, we multiply all distances with the same factor, until the estimated  $f$  is zero. Error bars shown throughout the paper are derived by varying the distance correction, until  $f$  is at the  $1\sigma$  confidence limit. The denominator of this term matters only for the error determination. The essential task is to find the distance correction factor, where  $\text{Cov}(W, y) = 0$ .

To construct an estimator, which is more stable against outliers in  $W$ , we cap the vertical velocities at  $|W| = 200 \text{ km s}^{-1}$ , i.e. assign all stars beyond that value the limit of  $\pm 200 \text{ km s}^{-1}$ . In statistical terms, we are essentially using an M-estimator for our linear regression. We have checked by varying this ceiling between 150 and  $400 \text{ km s}^{-1}$  that our results are not affected by outliers.

There are situations where sample kinematics are erroneous, or the data may be affected by streams. In this case it is useful to look at the separate statistics from the  $U \rightarrow W$  and  $V \rightarrow W$  terms. These separate terms have analogously the estimators:

$$f_V = \frac{\text{Cov}(W, T_{VW}V)}{\text{Var}(T_{VW}V) + < T_{VW}^2 \sigma_W^2 >} \quad , \text{ and} \quad (9)$$

$$f_U = \frac{\text{Cov}(W, T_{UW}U)}{\text{Var}(T_{UW}U) + < T_{UW}^2 \sigma_W^2 >} \quad . \quad (10)$$

#### 4.1 Bias corrections

There are three effects affecting the  $\text{Cov}$  term, and thus the distance estimator: the tipping of the velocity ellipsoid outside the Galactic plane, observational uncertainties in proper motions, and both  $v_{\text{los}}$  measurement errors and intrinsic  $v_{\text{los}}$  dispersion from binaries. We summarize the last two items as  $v_{\text{los}}$  source variance  $e_{\parallel}^2$ . To get an unbiased distance estimator we have to correct the measured covariance by:

$$\text{Cov}(W, T_{VW}V) = \text{Cov}_{\text{measured}}(W, T_{VW}V) - \text{Cov}_{\text{bias}}. \quad (11)$$

We now separate the bias term  $\text{Cov}_{\text{bias}}$  into its three sources: the bias from the tipping velocity ellipsoid  $\text{Cov}_{\text{ve}}$ , the measurement error on proper motions  $\text{Cov}_{\perp}$  and the  $e_{\parallel}$  term  $\text{Cov}_{\parallel}$ :

$$\text{Cov}_{\text{bias}}(W, T_{VW}V) = \text{Cov}_{\text{ve}} + \text{Cov}_{\perp} + \text{Cov}_{\parallel}. \quad (12)$$

Let us first discuss the minor term arising from the tipping of the velocity ellipsoid. As we can see in Fig. 2, some component of the galactocentric radial motion mixes into the heliocentric azimuthal velocity, when a star is observed away from the connecting line between Sun and Galactic centre. This way, the inclination of the non-isotropic velocity ellipsoid in galactocentric coordinates translates into a minor correlation between the velocities in the heliocentric frame. The velocity ellipsoid corrections from equations (40f.) of Schönrich et al. (2012) for the  $U \rightarrow W$  and  $V \rightarrow W$  terms read:

$$\begin{aligned} \text{Cov}_{\text{ve}}(W, T_{UW}U) &= \frac{1}{4} \left\langle \sin(2b) \cos(l) \cos(\alpha) \sin(2\beta) \left( \sigma_U^2 - \sigma_W^2 \right) \right\rangle, \\ \text{Cov}_{\text{ve}}(W, T_{VW}V) &= -\frac{1}{4} \left\langle \sin(2b) \sin(l) \sin(\alpha) \sin(2\beta) \left( \sigma_U^2 - \sigma_W^2 \right) \right\rangle, \end{aligned} \quad (13)$$

where  $\sigma_U^2$  and  $\sigma_W^2$ , are the radial and vertical velocity dispersions. For definitions of the angles, see Fig. 2 and Section 2.1. Here we assume that the velocity ellipsoid is pointing roughly towards the Galactic centre (Siebert et al. 2008; Binney et al. 2014).  $\sigma_U$  and  $\sigma_W$  are measured directly from the data. Since our samples are local and close to the plane (small  $\alpha$  and  $\beta$ ), the resulting bias on the distance estimators is significantly less than 0.01 for  $f_U$ , and less than 0.002 for  $f_V$ .

Adapting equations (23ff.) from SBA, we can calculate the bias in the covariance from proper motion errors:

$$\begin{aligned} \text{Cov}_{\perp}(W, T_{UW}U) &= -\sum_i T_{UW,i}^2 e_{\perp,i}^2, \\ \text{Cov}_{\perp}(W, T_{VW}V) &= -\sum_i T_{VW,i}^2 e_{\perp,i}^2 \end{aligned} \quad (14)$$

where again  $i$  is the index running over all stars in the sample.  $e_{\perp,i}$  is the uncertainty in the proper motion of star  $i$  in direction of the latitude  $b$ . If uncorrected, this term will feign a slight distance overestimate, but due to the excellent proper motions in TGAS, the resulting bias on the fractional distance error is below 0.3%.

#### 4.2 Line-of-sight velocity variance

The  $v_{\text{los}}$  errors require significantly more caution. Consider the effect on  $f_V$ , an analogous discussion will apply to  $f_U$ . Just where  $T_{VW}$  is maximal, i.e. at  $l \sim 90^\circ, 270^\circ$  and at an elevation of  $b \sim 45^\circ$  above the Galactic plane, an error in line-of-sight velocity determination will be evenly split into the derived  $V$  and  $W$  velocities, leading to a maximal correlation. This term will, if uncorrected, push the statistics towards a distance underestimate:

$$\begin{aligned} \text{Cov}_{\parallel}(W, T_{UW}U) &= \sum_i T_{UW,i}^2 e_{\parallel,i}^2, \text{ and} \\ \text{Cov}_{\parallel}(W, T_{VW}V) &= \sum_i T_{VW,i}^2 e_{\parallel,i}^2, \end{aligned} \quad (15)$$

where and  $e_{\parallel,i}^2$  is the source  $v_{\text{los}}$  variance (we analogously call  $e_{\parallel}$  the source  $v_{\text{los}}$  dispersion), i.e. all  $v_{\text{los}}$  variance that does not derive from the stellar velocity ellipsoid. For the full estimator  $f$  both  $\text{Cov}$  terms have to be added. We conceptually split  $e_{\parallel}$  into two contributions:

$$e_{\parallel}^2 = \sigma_{\text{los}}^2 + \sigma_{\text{bin}}^2, \quad (16)$$

where  $\sigma_{\text{los}}$  is the intrinsic measurement error in each survey, and  $\sigma_{\text{bin}}$  is the line-of-sight velocity dispersion from the orbital motion of multiple stellar systems (which we will address simply as “binary” contamination). The source  $v_{\text{los}}$  variance is the most important bias in LAMOST, with a distance bias near 10%. The impact of  $\sigma_{\text{los,RAVE}}$  on the distance estimators is nearly negligible with less than 0.3%, but  $\sigma_{\text{bin}}$  might be important. While the general problem of binary velocity dispersions has been known for a long-time (Olszewski et al. 1996; Hargreaves et al. 1996), we could not locate a good prediction for the Milky Way. A strong expected age-dependence (Gieles et al. 2010), and probably some metallicity dependence, make it difficult to translate results from dwarf spheroidal galaxies to the MW. Depending on the binary fraction and distribution, the dispersion contributed to the line-of-sight velocities could be of order  $3 \text{ km s}^{-1}$  with a large uncertainty (Vogt et al. 1995), though some open clusters appear to yield smaller values. This problem will be further examined in Sections 5.2 and 5.5.

Can we discriminate  $e_{\parallel}$  from a general distance error? To some extent, yes, with a sufficiently large number of stars in our sample. The bias from  $e_{\parallel}$ ,  $\text{Cov}_{\parallel}/N$ , for any sample of  $N$  stars should be the same between subsamples with the same geometry (i.e. distribution in values of  $T_{VW,i}$ ), and same  $v_{\text{los}}$  measurement quality and binary contamination (i.e. similar  $e_{\parallel,i}$ ). In contrast with this, the covariance term created by a distance error depends on the length of the baseline, which can be seen by isolating  $\text{Cov}(W, T_{VW}V)$  or  $\text{Cov}(W, y)$  in equation (8).

To summarize, these equations allow for a degenerate estimate between the mean distance error and an unknown bias in the line-of-sight velocities from binaries, but this degeneracy can be broken by selecting different subsamples with different baseline lengths  $\text{Var}(T_{VW}W)$ , either by cuts in metallicity or (more dangerous) by enforcing cuts on the galactocentric azimuthal velocity  $V_g$ .<sup>2</sup>

To account for uncertainties in  $\text{Cov}_{\text{bias}}$ , we add 30% of the distance bias from the tipping velocity ellipsoid and the proper motion errors as independent terms to the error budget in  $f$ . The geometric terms of the source  $v_{\text{los}}$  dispersion  $e_{\parallel}$  are not uncertain, and so we add 10% of this bias to the error budget.

### 4.3 Further biases and caveats

In a realistic galaxy, we expect further biases on our distance estimator from Galactic structure. The main features will be

- streams from accretion events,
- the Galactic warp correlating  $V$  and  $W$  motions near the line of nodes,
- (vertical) breathing modes from bar and spiral pattern, and
- disc streaming motions near resonances.

We do not expect a major bias from disc streaming, because those motions are predominantly in the galactic plane (Dehnen 2000; Pérez-Villegas et al. 2017), and our distance estimator is only biased by vertical motions.

Streams of accreted stars (see e.g. Kepley et al. 2007) show that a lot of the power of this method relies on mutual control of the different estimators and the spatial coverage. If a stream of accreted stars passes through the sample, it may have a large vertical motion  $W$ . This does not yet imply even a local bias on our distance estimator, because even a correlation between  $W$  and e.g.  $V$  velocities is not enough. The stream has to correlate  $W$  significantly with  $T_{VW}V$  to affect the  $f_V$  part. Even if the condition is fulfilled, good spatial coverage will cancel the bias to first order: If we have a bias at  $b > 0$ , an equivalent patch in the southern galactic hemisphere  $b < 0$  will cancel the impact of the stream, because the stream's  $W$  and  $V$  velocity will be similar, but the geometric term  $T_{VW}V$  reserves its sign. In addition, the  $f_U$  estimator will not be affected or react differently, and tend to cancel the effect. In short, streams on a sample with good

spatial coverage will not be a problem, and in worst case be detected by internal discrepancy between  $f_U$  and  $f_V$ .

Similarly, the Galactic warp may be a problem for the  $f_V$  term, but since the correlation between  $W$  and  $V$  will be similar in all directions (Dehnen 1998),  $f_V$  is only biased, if our sample looks predominantly into one quadrant of the sky. This is a major caveat, however, for dissecting samples in  $l$  and  $b$ .

Vertical breathing modes (Faure et al. 2014) are more dangerous, because their  $W$  motion reverses in parallel to a sign reversal of  $T_{VW}$  between  $b > 0$  and  $b < 0$ . This can have some impact, if the vertical motion feature is not symmetric in the field of view. However, the effect can be detected by comparing to the values from  $f_U$ .

A summary of performance tests of our method on N-body simulations of Milky-Way like galaxies, which reasonably match both Galactic structure and local kinematics, is discussed in the Appendix. On full sky samples measured at a solar-like position, the distance estimators perform at the level of their statistical error, i.e. the systematic effects discussed in this section must be below 1% on the distance estimator. The worst case scenario that we could find was a simulation with an unrealistically long bar. In that case the substructure introduced no concerning bias on the full sample, but a scatter of  $\sim 4\%$  in  $f_V$  and  $\sim 2\%$  in  $f$  when we restricted the sample to separate hemispheres in  $l$ .

We further note that  $f$  is an intrinsically quadratic estimator, as explained in SBA, i.e. the distance estimate is in fact  $f = 1 - \sqrt{\sum_i <(1 + f_i)^2 >}$ . This is caused by stars with distance overestimates having a longer measured baseline in  $y$ . The effect is not important here due to the good parallax quality in TGAS.

## 5 APPLICATION TO THE DATA

### 5.1 Mean distance error in the different subsamples

We start our discussion with an inventory of the mean distance biases in different subsamples, and will justify some of our assumptions in the later Sections. For deriving distances in these samples, we use the full distance prior from equation (1) including the survey selection functions, which we will derive in Section 5.3.1, and full bias corrections with the given errors according to equation (12).

Table 1 summarizes the distance statistics for different subsamples in RAVE and for LAMOST. The third column ( $\gamma$ ) provides the slope in the simple linear fit of  $W$  motion against  $VT_{VW}$  given in equation (7). These simple fits are shown with blue dashed lines for four samples in Fig. 3: all RAVE stars (top left), unflagged RAVE stars (top right), suspected binaries in RAVE (bottom left), and LAMOST (bottom right). These slopes indicate distance underestimates or significant  $v_{\text{los}}$  source dispersions  $e_{\parallel}$  in all samples, but in particular for the suspected binaries and LAMOST. The fourth and fifth columns of Table 1 show the two bias-corrected distance estimators  $f_V$  and  $f$  from equations (8) and (9). For the full RAVE sample, these terms both show a moderate, but significant distance underestimate of order 2%.

Our first, naive, idea was to ascribe this distance under-

<sup>2</sup> We iterate the warning that while it is feasible to cut the sample in  $V_g$ , cuts in heliocentric  $V$  are illicit, since they produce a biased cut in the actual velocity ellipsoid, biasing the sample in  $U_g$  and hence, via the inclination of the velocity ellipsoid in  $W$ .

**Table 1.** Distance correction factors assuming the given errors for different subsamples of RAVE and LAMOST stars. Column 2 shows the number of stars,  $\gamma$  is the slope in the simple linear regression from equation (7),  $f_V$  is the distance estimator from equation (9), and  $f$  is the full distance estimator from equation (8). The shorthands for the used samples are: RAVE: using RAVE stars with parallax errors better than 20%; RAVE<sub>10</sub>: RAVE stars with parallax errors better than 10%; all: all stars; nf: no flags; nf,s: no flags and excluding the distance region  $0.3 < s/\text{kpc} < 0.35$ ; b: at least one binary flag; LAMe1: LAMOST with given line-of-sight uncertainties  $\sigma_{\text{los,LAM}} < 25 \text{ km s}^{-1}$ , LAMe2: LAMOST with  $\sigma_{\text{los,LAM}} < 15 \text{ km s}^{-1}$ . A positive  $f$  indicates distances that are too long by a factor  $1 + f$ .

sample	# stars	$\gamma$	$f_V$	$f$
RAVE <sub>all</sub>	88513	$-0.039 \pm 0.007$	$-0.029 \pm 0.007$	$-0.015 \pm 0.005$
RAVE <sub>10,all</sub>	40589	$-0.063 \pm 0.010$	$-0.041 \pm 0.010$	$-0.024 \pm 0.007$
RAVE <sub>nf</sub>	59961	$-0.016 \pm 0.008$	$-0.012 \pm 0.009$	$-0.003 \pm 0.006$
RAVE <sub>10,nf</sub>	22587	$-0.027 \pm 0.014$	$-0.013 \pm 0.015$	$-0.009 \pm 0.009$
RAVE <sub>nf,s</sub>	53257	$-0.035 \pm 0.009$	$-0.026 \pm 0.009$	$-0.010 \pm 0.007$
RAVE <sub>b</sub>	5914	$-0.266 \pm 0.027$	$-0.174 \pm 0.024$	$-0.126 \pm 0.016$
RAVE <sub>10,b</sub>	2802	$-0.344 \pm 0.041$	$-0.215 \pm 0.037$	$-0.119 \pm 0.024$
LAMe1	28474	$-0.139 \pm 0.012$	$0.128 \pm 0.108$	$0.144 \pm 0.032$
LAMe2	6673	$-0.145 \pm 0.024$	$-0.016 \pm 0.040$	$0.009 \pm 0.018$

estimate to parallax errors in TGAS, as systematic effects are e.g. found in [Arenou et al. \(2017\)](#). However, when we select stars that have no flags according to [Matijević et al. \(2012\)](#), i.e. are considered likely normal stars, the distance bias diminishes. In turn, when we test suspected binary systems, i.e. stars that have at least one 'b' flag, there is a very strong bias equivalent to more than 10% distance underestimation. We can conclude from this that Gaia astrometry is generally of high quality, as long as we restrict the sample to apparently normal, single stars.

For the LAMOST sample, the situation is more complex. The simple linear regression test delivers a slope  $|\gamma|$  in excess of 0.1, i.e. a very strong kinematic bias. However, LAMOST  $v_{\text{los}}$  determinations have nominal measurement errors  $\sigma_{\text{los,LAM}} > 10 \text{ km s}^{-1}$ . Use the bias corrected statistics  $f$  and  $f_V$ , the expected bias fully accounts for this correlation in the LAMOST subsample with  $\sigma_{\text{los,LAM}} < 15 \text{ km s}^{-1}$ , resulting in a near-zero distance bias estimate. When we ease this limit to  $\sigma_{\text{los,LAM}} < 25 \text{ km s}^{-1}$ , the bias correction apparently overshoots, giving strongly positive  $f$ . The only viable conclusion is that LAMOST greatly overestimates its  $v_{\text{los}}$  measurement error. We will test this hypothesis and estimate the real  $v_{\text{los}}$  measurement error of LAMOST in the next section.

## 5.2 Testing line-of-sight velocity errors

We can use our method to test line-of-sight velocity errors. Even if we do not fully trust the parallax distances, Gaia-TGAS astrometry and hence our distance estimates are independent from the stellar parameters and line-of-sight velocity determinations. We can thus reasonably assume that the real distance bias in the sample should be nearly the same between samples of stars grouped according to their  $\sigma_{\text{los}}$  given by the spectroscopic surveys. A minor caveat is the potential correlations of line-of-sight velocity errors with stellar apparent magnitude, metallicities and ages, which introduce a small bias to the selection function.

The top panel of Fig. 4 shows the measured distance bias  $1 + f$  for subsamples of RAVE grouped by  $\sigma_{\text{los,RAVE}}$  and binned to samples of 4500 stars, sliding the mask by 1500 stars each, so every third data point is independent. We use the given error estimates from the RAVE pipeline, i.e. we set  $e_{\parallel} = \sigma_{\text{los,RAVE}}$ . The expected bias correction on the dis-

tance statistics from  $\sigma_{\text{los}}$  is small in this region, reaching  $\delta f \sim 1.5\%$  at  $e_{\parallel} = 5 \text{ km s}^{-1}$ . Green errorbars show the statistics for the entire RAVE sample, while the blue error bars depict the unflagged RAVE sample, again using the flags from [Matijević et al. \(2012\)](#). There are some stars in the RAVE sample with given  $\sigma_{\text{los,RAVE}} > 10 \text{ km s}^{-1}$ , and the sharp decline in the  $1 + f$  estimate seen in the full sample continues for those. Since their distance error should not be substantially different, this implies that beyond  $\sigma_{\text{los,RAVE}} > 5 \text{ km s}^{-1}$ ,  $v_{\text{los}}$  estimates are significantly more uncertain than stated and should not be used at all. It is apparent that the unflagged sample shows excellent stability; the little aberration around  $\sigma_{\text{los,RAVE}} \sim 1.7 \text{ km s}^{-1}$  is likely just a statistical fluctuation (about 10 error bars should have their  $1\sigma$  confidence intervals not crossing 1.0). The entire sample, however, shows a clear abnormality for  $\sigma_{\text{los,RAVE}} > 2 \text{ km s}^{-1}$ . Apparently the flagged stars contain line-of-sight velocity uncertainties beyond the provided errors, but the contamination is comparably small for  $\sigma_{\text{los,RAVE}} < 2 \text{ km s}^{-1}$ . There is some tentative indication for problems with the line-of-sight velocities of stars with very small errors  $\sigma_{\text{los,RAVE}} < 0.7 \text{ km s}^{-1}$ , possibly from some erroneous  $\sigma_{\text{los,RAVE}}$  determinations going in hand with  $v_{\text{los}}$  measurement errors.

The same analysis on LAMOST (bottom panel of Fig. 4) shows how useful this method can be. Note that the x-axis in this plot just starts beyond the range of the top panel, i.e. in the entire sample, the correction of  $f$  for  $e_{\parallel}$  and hence  $v_{\text{los}}$  errors is crucial. Here, we show the bias corrected estimates for  $1 + f$  with red error bars, setting  $e_{\parallel} = \sigma_{\text{los,LAM}}$ . These are compared to the same estimate without correcting for the  $e_{\parallel}$  bias. If the pipeline estimates for  $\sigma_{\text{los,LAM}}$  were correct, the red errorbars should lie in a horizontal line, while the uncorrected estimates (blue) should trend sharply downwards. However, we observe the opposite. While the uncorrected  $1 + f < 1$  indicates a significant  $v_{\text{los}}$  source dispersion  $e_{\parallel}$ , the points lie in a horizontal line, indicating that there is almost no correlation between the real  $e_{\parallel}$  and the estimated  $\sigma_{\text{los,LAM}}$ . We conclude that  $\sigma_{\text{los,LAM}}$  does not indicate the real  $v_{\text{los}}$  measurement error, and that the real  $v_{\text{los}}$  measurement errors must be far better than claimed by their pipeline. In accordance with this, the red errorbars trend sharply upwards, because the bias correction increasingly overestimates the real  $v_{\text{los}}$  measurement uncertainty, explaining our findings in Table 1.

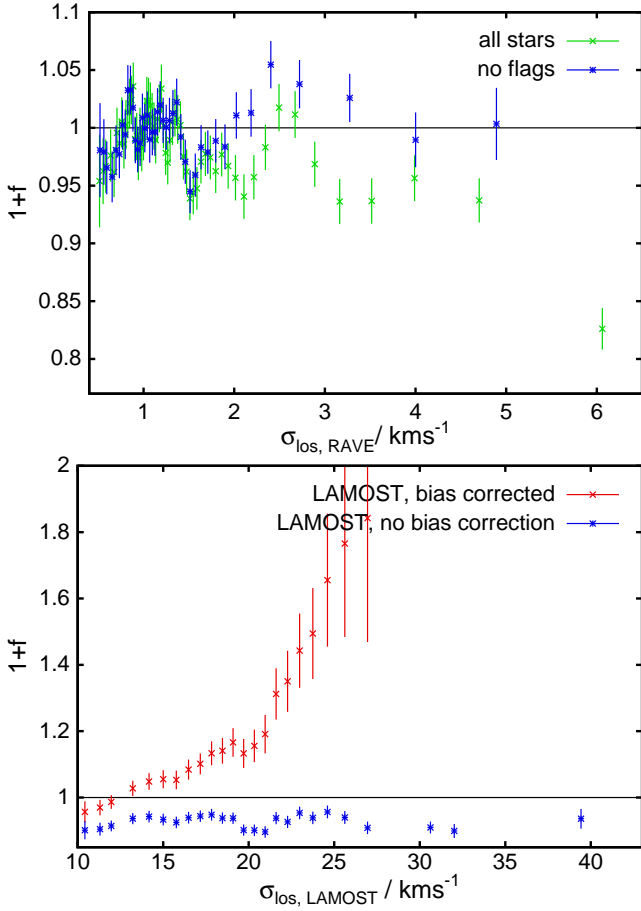


**Figure 4.** Testing line-of-sight velocity uncertainties  $\sigma_{\text{los}}$  as provided by the RAVE (top panel) and LAMOST surveys (bottom panel). Both samples were binned in  $\sigma_{\text{los}}$  using a mask of 4500 stars sliding by steps of 1500 stars, so every third data point is independent. For RAVE the velocity errors are generally very small, resulting in very small bias corrections, and we provide in this plot only bias corrected estimates. The entire RAVE sample is shown with green error bars, the subsample of unflagged stars is shown in blue. Note the better stability of the cleaned sample, towards larger  $\sigma_{\text{los}}$ . Due to the larger errors in LAMOST, the bottom plot is on a different scale. Here we plot the bias corrected distance statistics (red error bars) vs. the uncorrected distance statistics (blue). The last data points for the corrected sample are above the figure margin.

**Table 2.** Fit parameters for testing the line-of-sight velocities via the dependence of vertical velocities on  $\sin(b)$  as in equation (17). The slope  $\xi$  between  $W$  and  $\sin(b)$  can be interpreted as an average  $v_{\text{los}}$  measurement offset  $\delta v_{\text{los}}$ .

sample	$\delta v_{\text{los}} / \text{km s}^{-1}$	$-W_0 / \text{km s}^{-1}$
RAVE <sub>all</sub>	$0.26 \pm 0.13$	$-7.67 \pm 0.09$
RAVE <sub>nf</sub>	$0.23 \pm 0.16$	$-7.55 \pm 0.10$
RAVE <sub>10,nf</sub>	$-0.04 \pm 0.26$	$-7.98 \pm 0.17$
RAVE <sub>b</sub>	$0.19 \pm 0.47$	$-8.26 \pm 0.31$
LAMOST	$-4.82 \pm 0.20$	$-7.62 \pm 0.14$
LAMOST <sub>e15</sub>	$-4.75 \pm 0.40$	$-7.71 \pm 0.29$

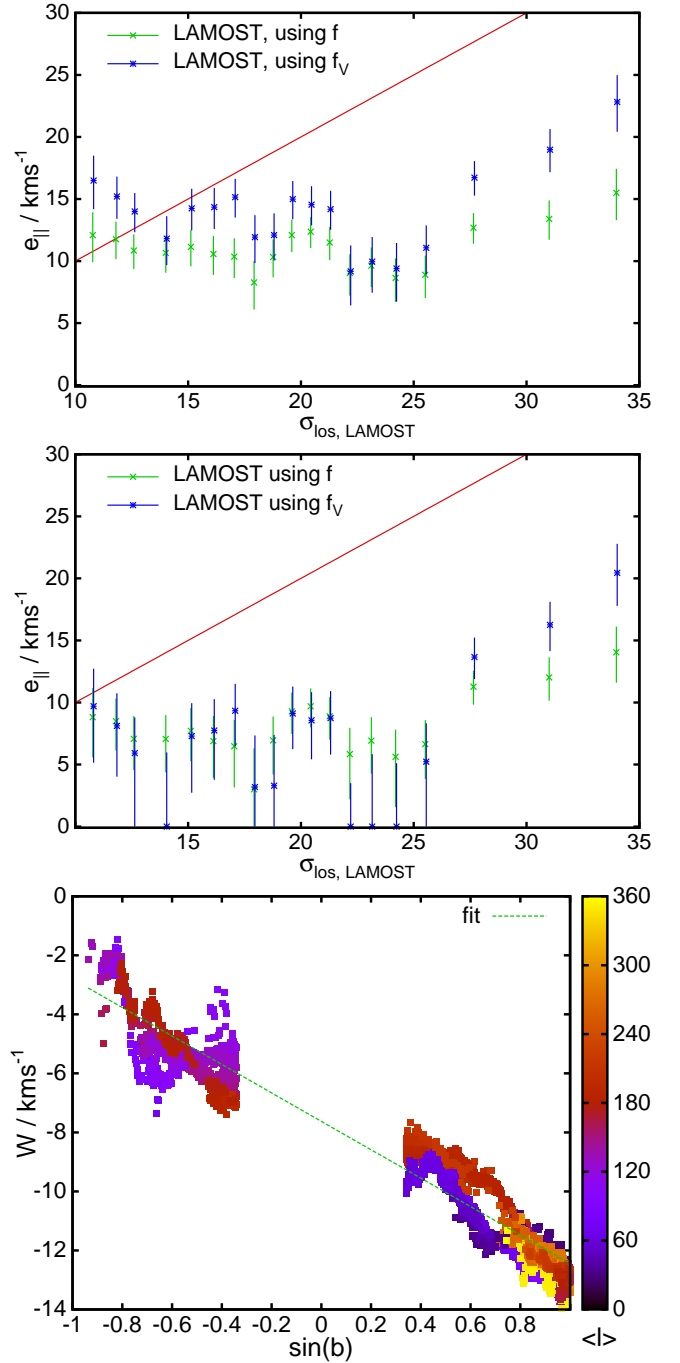


**Figure 5.** Top panel: Measuring the  $v_{\text{los}}$  source dispersion  $e_{\parallel}$  in subsamples of stars ordered by the measurement uncertainty as provided by LAMOST in each subsample. Since for these values  $e_{\parallel}^2 \gg \sigma_{\text{bin}}$ , the values on the y-axis can be directly compared to  $\sigma_{\text{los,LAM}}$ . We mark the identity line in black. The plot uses again a sliding mask, i.e. every third datapoint is independent. In the middle panel, we show the same statistics, but using a general correction of LAMOST  $v_{\text{los}}$  by the offset  $\delta v_{\text{los}} = 5 \text{ km s}^{-1}$ . The bottom panel shows the average vertical velocity  $W$  vs. average  $\sin b$  when we take around each star all objects with  $\sin b$  values within 0.1 and longitude  $l$  within  $\pi/4$ . The trend-line (green dashed) was obtained by fitting equation (17) on the LAMOST sample; it's slope indicates a  $5 \text{ km s}^{-1}$  global bias in LAMOST  $v_{\text{los}}$  measurements, which we corrected to create the middle panel.

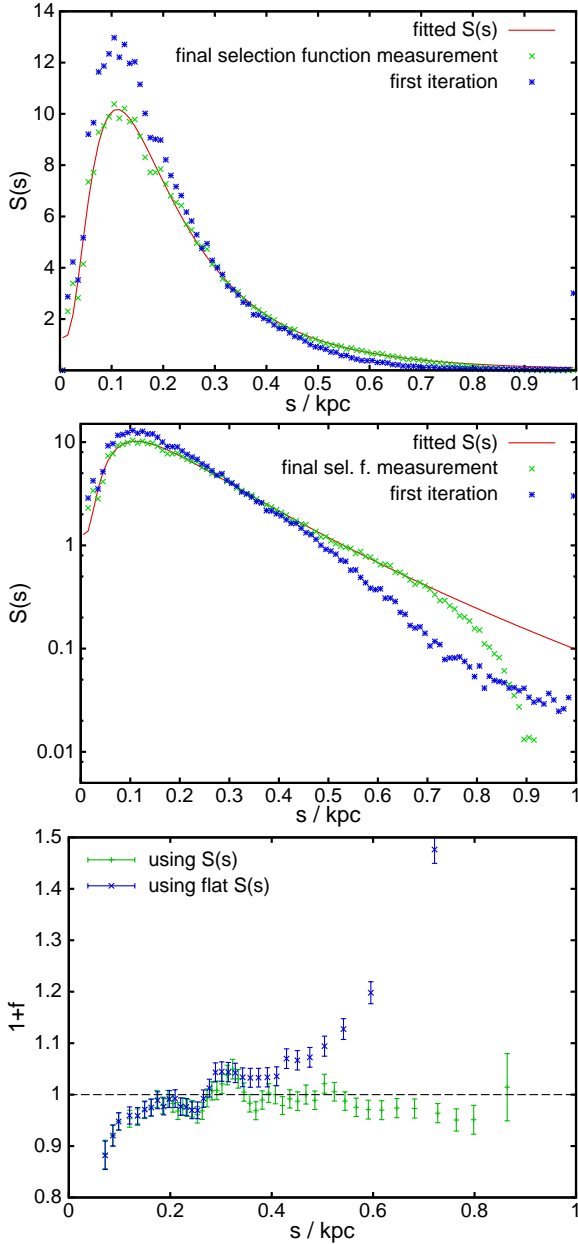


**Figure 6.** Derivation of the RAVE selection function using the entire RAVE-TGAS sample, the top panel in linear scale, the middle panel in log-scale. The blue points show the first measurement for  $S(s)$  when starting with a trial flat selection function. The selection function  $S(s)$  converges as shown within less than 5 iterations to its final value. The red line gives the smooth fitting function applied. The break-down of the selection function on the right-hand end of the distribution is caused by the quality cuts on the parallax accuracy, not to be fitted. The bottom panel compares the distance statistics between using the final  $S(s)$  (green) and a flat  $S(s)$  (blue) binned in  $\langle s \rangle$ . The last (blue) data points in the flat  $S(s)$  are not shown as they have  $1 + f > 2$ .

The top panel of Fig. 5 shows the measurement of  $e_{\parallel}$  from the bias in  $f$  when ordering the sample in terms of  $\sigma_{\text{los,LAM}}$ . For this figure, we use our experience from RAVE that the distance bias should be negligible compared to the  $e_{\parallel}$  bias correction, and hence determine  $e_{\parallel}$  by demanding an estimate of  $f = 0$  after the bias correction. The error bars

are derived by varying  $e_{\parallel}$  until the estimate for  $f$  becomes marginally positive or negative. Since the bias correction on  $f$  from equation (15) is quadratic in  $e_{\parallel}$ , the error bars on  $e_{\parallel}$  are asymmetric. The plot clearly shows that  $e_{\parallel}$  is nearly uncorrelated with  $\sigma_{\text{los,LAM}}$ , in fact it slightly declines. The sudden rise of  $e_{\parallel}$  near  $\sigma_{\text{los,LAM}} = 27 \text{ km s}^{-1}$  indicates problems with  $v_{\text{los}}$  estimates beyond this point, so that we from now on will adopt the quality cut  $\sigma_{\text{los,LAM}} < 27 \text{ km s}^{-1}$ . However, there is a problem: The estimates of  $e_{\parallel}$  using the full set of terms in  $f$  are significantly smaller than the estimates of  $e_{\parallel}$  when using only the azimuthal vs. vertical motions in  $f_{\nu}$ . Something must be wrong beyond a random uncertainty.

The bottom panel of Fig. 5 solves this riddle. Around each star in LAMOST we select all stars that have a similar value in galactic latitude, i.e.  $\Delta \sin(b) < 0.1$  and lie within  $\pi/4$  in  $l$ . We plot the average vertical velocity of each subsample vs. its mean value in  $\sin(b)$ ; the colour indicates the mean longitude  $\langle l \rangle$  in degrees. Apart from some statistical fluctuations, the sample lies almost perfectly along a line:

$$W = -W_{\odot} + \xi \sin(b). \quad (17)$$

However,  $\sin(b)$  is just the projection factor of the  $v_{\text{los}}$  estimate into  $W$ , so the slope  $\xi$  can be interpreted as an average global offset in the  $v_{\text{los}}$  determinations:  $\xi = \delta v_{\text{los}}$ . An alternative explanation would be a vertical breathing mode in the disc, but it cannot explain the perfect trend. Table 2 compares fits of equation (17) for different subsamples of RAVE and LAMOST. No subsample of RAVE shows an appreciable slope, ruling out a physical phenomenon. We conclude that LAMOST has a bias of  $\delta v_{\text{los}} \sim -5 \text{ km s}^{-1}$ , which we correct by adding  $5 \text{ km s}^{-1}$  to all LAMOST  $v_{\text{los}}$  estimates.

The middle panel of Fig. 5 confirms the benefit of this correction - the two different estimators for  $e_{\parallel}$  are now in line. The estimated  $v_{\text{los}}$  source dispersion  $e_{\parallel} \sim 7.2 \text{ km s}^{-1}$  is significantly smaller than in the top panel, and shows that the LAMOST  $v_{\text{los}}$  determinations are far more precise than their estimate  $\sigma_{\text{los,LAM}}$ . We also find a comparable dichotomy of mean radial stellar velocities inwards and outwards along the connection line between Sun and Galactic Centre, which confirms the  $v_{\text{los}}$  offset found on vertical motion. Such an offset in  $v_{\text{los}}$  is not unprecedented - SEGUE/SDSS was plagued by a similar offset, and even after its correction, Schönrich (2012) found a residual bias, although smaller than this one. The fact that the  $v_{\text{los}}$  bias on SEGUE depends on colour and metallicity of stars as discussed by Schönrich (2012), indicates that a future revision of the LAMOST sample should examine those dependencies as well.

To summarize our findings in this Section: We have shown that our method can be used to test the quality of  $\sigma_{\text{los}}$  estimates.  $v_{\text{los}}$  estimates and  $\sigma_{\text{los,RAVE}}$  estimates from the RAVE survey are of high quality, with minor issues for flagged stars. A strict cut of  $\sigma_{\text{los,RAVE}} < 5 \text{ km s}^{-1}$  should be applied. The LAMOST  $v_{\text{los}}$  determinations are far more precise than suggested by their nominal  $\sigma_{\text{los,LAM}}$ . We adopt the quality cut  $\sigma_{\text{los,LAM}} < 27 \text{ km s}^{-1}$ . One should adopt a general error of  $\sigma_{\text{los}} \sim 7.2 \text{ km s}^{-1}$ , and correct all  $v_{\text{los}}$  estimates by  $+5 \text{ km s}^{-1}$ .

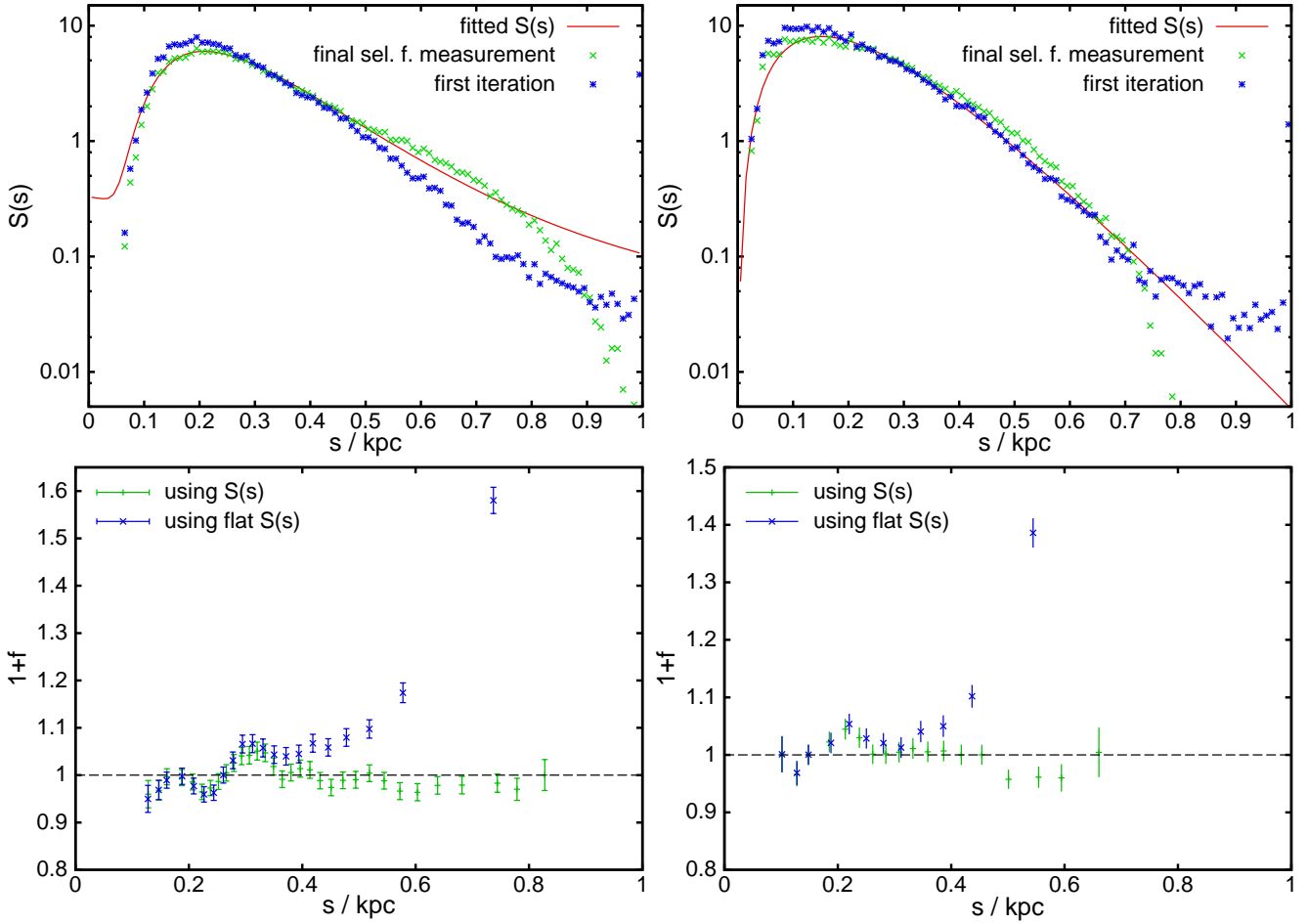


**Figure 7.** Same as Fig. 6, for RAVE-TGAS stars that are unflagged (left column) and LAMOST (right column). When calculating the distance statistics (bottom row) we apply all bias corrections in RAVE, but no bias corrections in LAMOST. The last data points in the flat  $S(s)$  are not shown because they are far above the range of this plot.

### 5.3 Distance dependent bias

#### 5.3.1 Retrieving the prior/selection function

In this section we will finally derive the selection function  $S(s)$  required in the distance estimate in equation (1) and test it by measuring the distance bias  $f$  in samples binned in distance  $s$ .

A full a priori calculation of the distance priors and selection functions  $S(s)$ , which enter the distance estimation in equation (1), would demand a full chemodynamical model of the disc with all its assumptions. Population synthesis models can calculate  $S(s, \tau, [\text{Fe}/\text{H}])$  and give us some indication of the shape of the selection function. However, even with this knowledge, we still cannot reliably build a selection function for our samples, since we would need to know/assume the exact distribution of stars in age and metallicity at each point in the Solar neighbourhood.

For example, the RAVE selection function described in Wojno et al. (2016) can be roughly described as a flat selection in I-band magnitudes between about 9 and 11.3 mag, with some wings towards lower and higher magnitudes. Running a population synthesis model as used in Schönrich & Bergemann (2014) on this selection, demanding additionally  $T_{\text{eff}} > 4200$  K for reasonable stellar param-

eter estimates, we obtain a relatively steep selection function  $S(s, \tau)$  in distance and age:  $S(s)$  at fixed metallicity and age falls off approximately exponentially with a scale-length of 0.12 kpc at  $s > 0.2$  kpc, and with a flatter slope at  $s > 0.5$  kpc. At fixed metallicity and distance  $S(\tau)$  behaves roughly like  $1/(\tau + 1.5)$  Gyr.

Here, we will adopt a simpler, more direct approach: we can actually derive the  $S(s)$  from the data. We know that with the correct prior, this should give stable values of  $f$  vs.  $\langle s \rangle$ , just like we could demand a stable distance bias  $f$  when binning in  $\sigma_{10s}$  in the previous section.

To obtain the full prior including the selection function, we start from the simple density model in equation (3). For the sake of simplicity, we assume that the selection function is solely a function of distance, i.e.  $S(s)$ , ignoring angle-dependent deviations from the simple density model, and more importantly from the age- and metallicity structure of the disc. We can now measure  $S(s)$  in a simple way: With an expected distribution of stars in distance  $\rho_S(s)$ , we can estimate  $S(s) \sim \rho_m(s)/\rho_S(s)$ , where  $\rho_m(s)$  is the measured density of stars in distance. Since the distances of single stars are quite well-determined, we approximate  $\rho_m(s)$  by simply binning the number of stars according to their distance expectation value  $\langle s \rangle$ . One caveat is that near the far end of

the sample, the measurement will fall quickly below the real selection function, due to stars dropping out from the sample by the quality cut on parallax accuracy. The latter information is already used by the quality cut, and so must not be written into the prior.

To obtain  $\rho_S(s)$  we use the positions  $(l_i, b_i)$  on the sky of all stars  $i$  in the sample on our density model and sum up their normalised density distributions in distance  $s$ :

$$\rho_S(s) = \sum_i N'_i s^2 \rho(s, l_i, b_i), \quad (18)$$

where

$$N'_i{}^{-1} = \int ds s^2 \rho(s, l_i, b_i) \quad (19)$$

normalises the integral in distance  $s$  over each of the individual distance distributions to 1, and  $\rho(s, l_i, b_i)$  is calculated from equation (3). The problem is solved by an iteration. We start with a flat  $S_0(s)$  in distance, calculate all distance expectation values from equation (1), bin them in distance to obtain  $\rho_m(s)$  and calculate our first estimate for  $S_1(s) = \rho_m(s)/\rho_S(s)$ . We fit  $S_i(s)$  with a simple analytic equation. A smooth fitting function is important, because a non-smooth function might pull data towards single points yielding a false convergence. We re-insert this analytic approximation to  $S$  into the distance calculation and repeat the procedure, until the selection function converges (typically within five iterations).

The top (linear) and middle (logarithmic plot) panel of Fig. 6 show the measurement and fits to the selection function from the entire RAVE sample. The blue points show the first estimate  $S_1(s)$ , and green points depict the final estimate for  $S(s)$ , which is the selection function that reproduces itself in further iterations. The precise parallaxes on the near end result in virtually no change of the shape of  $S$  at distances  $s < 0.2$  kpc. On the long distance end, the selection function pulls stars closer, steepening  $S(s)$ .

As a fitting equation we employ a log-normal distribution, plus a minor exponential term to smooth the edges:

$$S(s) = d_1 (\exp(-((\ln(s/\text{kpc}) - \ln(a))c_1)^2/2) + d_2 \exp(-sc_2)), \quad (20)$$

where  $a, c_1, c_2, d_1, d_2$  are free fitting parameters. The fit shown in Fig. 6 yielded  $a = 0.1135, c_1 = 1.402, d_1 = 9.440, d_2 = 0.1379, c_2 = 5.062 \text{ kpc}^{-1}$ , converging within five iterations. The fit quality is good; the discrepancy at large  $s$  is caused by the quality cut on parallaxes, which must not be part of  $S(s)$ .

### 5.3.2 Testing the selection function

Beyond this good convergence of  $S(s)$ , how can we judge if this selection function is reasonable? The key lies again in the distance statistics. The bottom panel in Fig. 6 shows  $1+f$  on the y-axis, using either a flat  $S$  (blue errorbars), or the derived  $S(s)$  from equation (20), depicted in green errorbars. At the far end of the sample, where parallaxes are relatively uncertain, a flat selection function results in a massive overestimate of stellar distances, which in turn gets signalled by  $1+f \gg 1$  in the blue errorbars. The last data points for the flat  $S(s)$  are not shown, because they have  $1+f > 2$ , outside the plotting range. The declining

parallax precision hence results in a strong trend in  $f$ , while with the (relatively) correct selection function, we see no such trend. This is direct proof that the selection function is sound and has to be applied. Note that when binning in  $1/p$ , the breakdown in the distance statistics for a flat  $S(s)$  would be found in almost all of the sample with  $p \lesssim 5 \text{ mas}$ .

The left-hand column of Fig. 7 shows the same results for the RAVE-TGAS sample when selecting only unflagged stars (left column). The fitting parameters for the RAVE selection function (equation 20) are  $a = 0.2087, c_1 = 2.055, d_1 = 9.440, d_2 = 0.03626, c_2 = 1.5 \text{ kpc}^{-1}$ . The exponential scale-length is fully degenerate with the normalisation of the exponential term, and is hence undetermined by the fit. However, it has a significant impact on the long-range behaviour of  $1+f$ : if we would use  $e \lesssim 1.5$ , i.e. a scale-length of the selection function larger than about  $0.7 \text{ kpc}$ ,  $1+f$  would become significantly larger than 1 for  $s > 0.6 \text{ kpc}$ . The chosen value of  $e = 1.5$  is in the range predicted by population synthesis models, and a compromise between our distance statistics and the direct fit for  $S(s)$ , and leads to a satisfactory result in the bottom left panel of Fig. 7.

On the right-hand side of Fig. 7 we analyse the selection function of the LAMOST survey. This selection function is not only limited by the survey's magnitude cuts, but also by our applied signal-to-noise limit of  $\text{SNR} > 30$  in the r-band. The LAMOST selection function could not be fitted by the same log-normal distribution as RAVE, so we choose

$$S_L(s) = as^2 \exp(-cs), \quad (21)$$

where the free-fit parameters are determined as  $a = 2593.38 \text{ kpc}^{-2}, c = 13.21 \text{ kpc}^{-1}$ . The fit is not good for small  $s < 0.1 \text{ kpc}$ , since we made no attempt to fit the distribution in that range. As detailed above,  $S$  plays a negligible role for determining distances at  $s < 0.1 \text{ kpc}$  due to the high quality of TGAS parallaxes. On the right-hand side there is a small bump in both the RAVE unflagged sample and in the LAMOST sample compared to our fits. Since the selection function only has to capture the rough shape of the distribution, this is acceptable. Also, the distance statistics in the bottom panel indicate that we cannot allow for a steeper decline in  $S(s)$  at  $s > 0.5 \text{ kpc}$ , since this would make the distance underestimate in this region significant.

### 5.3.3 Nature's bad joke: The simple parallax estimator

Fig. 8 shows the estimated  $1+f$  distance estimator vs.  $s'$  for the RAVE-TGAS sample (top panel) and the LAMOST sample (middle panel), when we use the naive estimate  $s' = 1/p$  instead of the full distance estimate from equation (1). These statistics look surprisingly good. While the general distance underestimate in RAVE gets slightly worse and there is a trend towards small  $1+f$  at large  $s'$ , but the naive estimate obviously avoids the catastrophic failure we registered when neglecting the selection function, as shown in Fig. 6 and Fig. 7.

Already Strömberg (1927) pointed out that one should be careful not to use  $s' = 1/p$  blindly, but by a mood of nature, or rather the selection function, the resulting distance bias in these samples is quite small. We would expect a gradual increase of the bias towards larger distances, where the parallax quality decreases, just like it happened with  $1+f$  vs. distance, when we used the flat selection function  $S(s)$  in

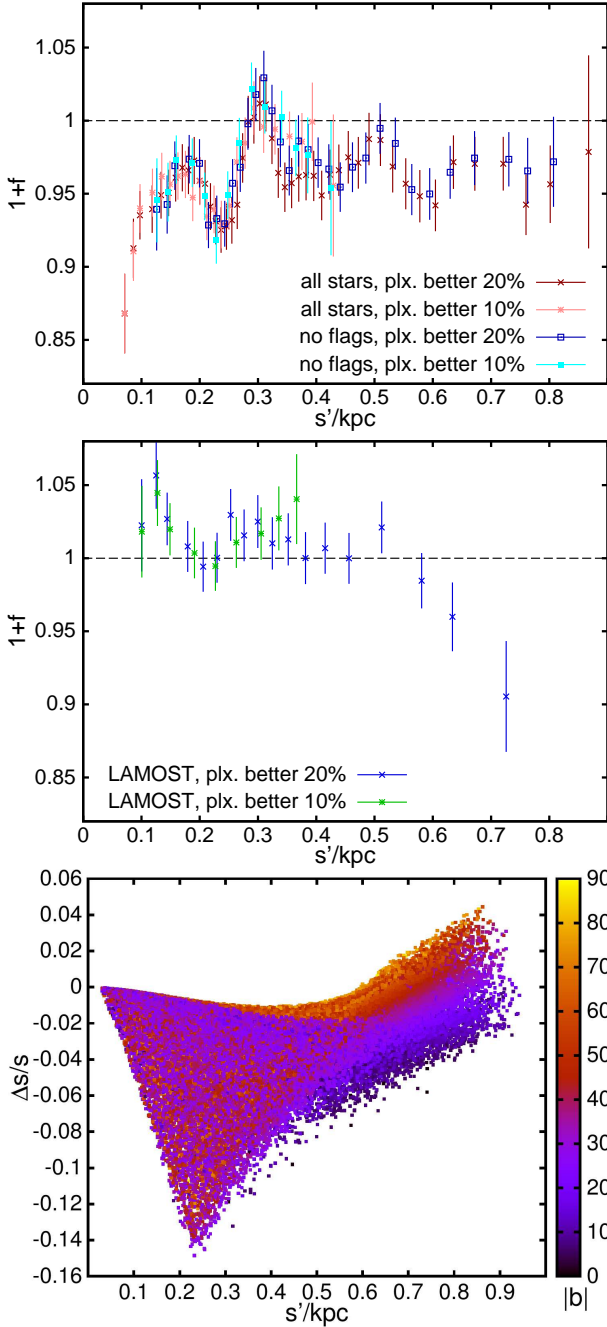


**Figure 8.** Distance statistics when using the simple  $s' = 1/p$  distance estimator for RAVE (top panel) and LAMOST (middle panel). The distance statistics for LAMOST are balanced, since we use  $e_{\parallel} = 7.2 \text{ km s}^{-1}$ . The bottom panel shows for RAVE stars with  $\sigma_p/p < 20\%$  the relative difference  $\Delta s/\langle s \rangle = (s' - \langle s \rangle)/\langle s \rangle$  between the full distance estimate  $\langle s \rangle$  from equation (1) and  $s' = 1/p$  coloured by the absolute  $|b|$ .

the previous section. Yet, for RAVE-TGAS  $1+f$  is remarkably stable. This is achieved because the selection function in RAVE almost perfectly cancels the terms from the coordinate transformation and the density distribution (the selection function falls steeply in distance, acting in the same direction as the  $s'$  estimate). The LAMOST sample shows good stability out to about 0.5 kpc.

The cancellation of the distance biases is also evident

from the bottom panel of Fig. 8, where we plot for the full RAVE sample with parallaxes better than 20% the relative difference in the distance estimates  $\Delta s/\langle s \rangle = (\langle s \rangle - s')/\langle s \rangle$  for each star.  $\langle s \rangle$  is the full distance estimate using equation (1). The datapoints are coloured by their galactic latitude  $|b|$ . Since the density falls quicker towards higher latitudes, the distance underestimate by  $s'$  is stronger for stars at small latitude  $|b|$ . To understand the shape of this plot, we remember the behaviour of the RAVE selection function from equation (20) and the top panel of Fig. 6. At distances below  $\sim 0.2$  kpc the selection function is rising and  $s^2\rho_S(s)$  rises sharply as well, so that stars with even moderate parallax uncertainty show a strongly negative  $\Delta s/\langle s \rangle$ . However, beyond that point, the selection function and the spatial density fall steeply, bringing  $s'$  closer to the full estimate. As a result, the average  $\Delta s/\langle s \rangle$  is about  $-2.4\%$  in the RAVE sample with parallaxes better than 20% ( $\sigma_p < 0.2p$ ), and  $-1.4\%$  in the sample with parallaxes better than 10%.

#### 5.4 A bump in the distance statistics

The top panel of Fig. 9 shows the distance estimator  $1+f$  when binning stars in the RAVE sample according to their distance  $\langle s \rangle$  in bins of 6000 stars each. Both sample selections of the RAVE-TGAS sample (red error bars: all stars, green error bars: unflagged stars) display a marked peak in  $1+f$  around  $s \sim 0.3$  kpc. The feature is very narrow, and mostly limited by the distance accuracy and our ability to sample around it. It is stronger than we would expect to be possible for a statistical fluctuation, and we have checked that changes in the adopted selection function do not alter this result. In addition, an increase of the parallax accuracy does not remove the feature, even if we use  $\sigma_p/p < 10\%$ . We can exclude that this is a global issue with the parallax measurements, since the LAMOST survey in the opposite direction of the sky does not show this signal.

In the middle and bottom panels of Fig. 9 we try to dissect the sample further to find the origin of this feature. As we have discussed in Section 4.3, separating the different parts of the distance estimator, and in particular separating the sample in longitude or latitude make the analysis more prone to impacts by Galactic substructure. The middle panel compares the full estimator to its restricted counterparts from equation (9) which exclusively use the azimuthal velocity component ( $f_V$ , blue) or the radial velocity component ( $f_U$ , green). The peak around  $s = 0.3$  kpc is stronger in  $f_V$  than in  $f_U$ , though both estimators show a distance overestimate. The bottom panel attempts to dissect the sample in longitude  $l$ . This is not a safe selection, and likely the general downtrend seen in  $l$  is a consequence of the Galactic warp (the warp correlates  $W$  and  $V$ , since the sample is mostly at  $b < 0$  and  $T_{VW}$  changes sign at  $l = 180^\circ$ ,  $f_V$  should change sign at this point). However, again the stars between  $s = 0.3$  and 0.35 kpc show a markedly different behaviour. Attempts to further narrow the origin of this feature revealed that the signal is coming from around  $l \sim 300^\circ$  and latitudes both above and below the Galactic plane. This position corresponds roughly to  $\text{RA} \sim 185^\circ$  and  $\text{DEC} = -60^\circ$ . Detailed inspection of the kinematics did not reveal any evident stream at this position. Also, a stream passing through could correlate  $W$  and  $V$  motions, but the sign of  $T_{VW}$  changes with the sign change in latitude  $b$ , and so  $f$  should reverse sign

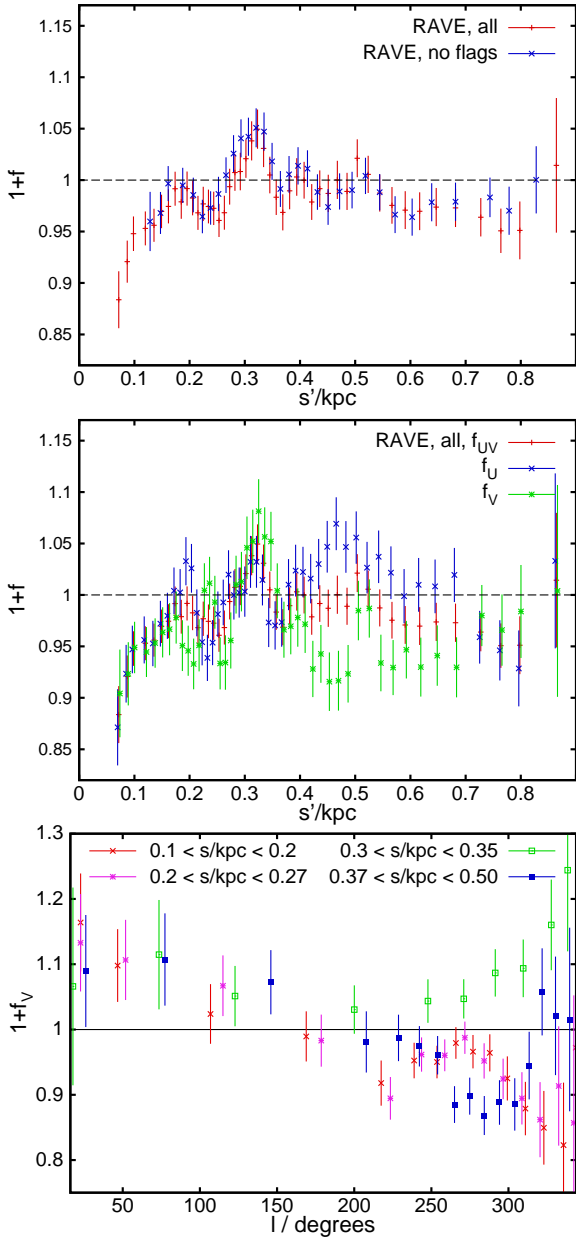


**Figure 9.** Top panel: comparing the distance statistics for RAVE stars, when binning in distance to samples of 6000 stars each, sliding the mask in steps of 2000 stars. Middle panel: Comparing the full distance estimator  $1+f$  (red) to the restricted estimators using only the radial  $f_U$  (green), or the azimuthal  $f_V$  (blue) velocity components. Bottom panel: Dissection of the distance statistics vs. Galactic longitude  $l$  in the RAVE sample at different heliocentric distances  $s$ .

as well, which it does not. Consistently, kinematic cuts to remove eventual outliers in  $W$  do not remove the feature. We have checked that the bias corrections are more than an order of magnitude too small to account for this deviation, i.e. even a large mistake in our assumptions can not explain the feature. We have further drawn exclusion zones of  $7^\circ$  around the positions of the Magellanic clouds and found no difference in the values of  $f$ . A vertical breathing mode in the disc would be the only possibility that we could currently imagine to give rise to this feature, and the reversal of  $f_V$  to

distances of  $s > 0.4$  kpc could be interpreted as the location of a spiral arm or spur. However, there is no known spiral arm in this region. The next feature in this direction would be the Sagittarius/Carina arm, which is more than a kpc away (see e.g. Reid et al. 2014). In addition to the distance discrepancy the explanation by a spiral arm/spur would also raise the question how this feature can be so narrow/sharp in distance.

We also note that all RAVE samples show a distance underestimate for stars with  $s < 0.15$  kpc. The parallaxes at this short distance are nominally too good to allow for such an effect by a wrong choice of the selection function  $S(s)$ . We think that this is either an extreme statistical outlier, or there is a problem in TGAS with large parallaxes and/or the bias against stars with large proper motions is significantly more severe than we take from the precaution in Lindegren et al. (2016).

To summarize this: the most likely conclusion is that there is a problem with TGAS parallaxes near  $l \sim 300^\circ$  and distances of  $0.32 \pm 0.03$  kpc ( $p \sim 3$  mas). If it is not a glitch in the data, the feature is unlikely to be a stream. However, it might be related to disc structure. Since our estimate correlates azimuthal and vertical velocities, this cannot be a pure in-plane feature, though the location would rather point to a not yet established interarm, or spur. This feature warrants tests of the Gaia pipeline, and it should be investigated as a possible place for Galactic substructure.

## 5.5 Assessing the source $v_{\text{los}}$ dispersion: LAMOST

We now return back to the question of the source  $v_{\text{los}}$  dispersion  $e_{\parallel}$  and ways to differentiate it from parallax errors. As discussed above, the bias term in equations (12, 15) can be used to measure  $e_{\parallel}^2$ , if the distance bias  $f$  in a sample is sufficiently well-constrained.

This works very well e.g. for the LAMOST dataset. In this case the parallaxes and our method to retrieve the selection function and distance priors have been validated on the RAVE sample to an accuracy better than 2%. The source  $v_{\text{los}}$  dispersion  $e_{\parallel}$  can now be determined by plotting the corrected distance bias estimate  $1+f$ , while varying the source  $v_{\text{los}}$  dispersion  $e_{\parallel}$ . This is done in Fig. 10, where the green lines show this variation for the LAMOST sample, dashed lines represent the  $1\sigma$  error intervals. We use the quality cuts derived in Section 5.2,  $\text{SNR} > 30$  and  $\sigma_{\text{los,LAM}} < 27 \text{ km s}^{-1}$ , however, do not use  $\sigma_{\text{los,LAM}}$  in the bias correction of  $1+f$ . Under the assumption that the distance estimates from TGAS parallaxes are unbiased, we obtain  $e_{\parallel} = 7.2 \pm 1.0 \text{ km s}^{-1}$ . This estimate contains a generous allowance for uncertainties in the velocity ellipsoid and proper motions. The systematic uncertainty from the distances is difficult to estimate, but from the previous indications it should be of order  $2 \text{ km s}^{-1}$ .  $e_{\parallel}$  consists of the  $\sigma_{\text{los}}$  and additional source dispersion from binary systems. However, the latter should be of order  $\sigma_{\text{bin}} \lesssim 3 \text{ km s}^{-1}$ , so according to equation (16), their contribution to  $e_{\parallel}$  is small.

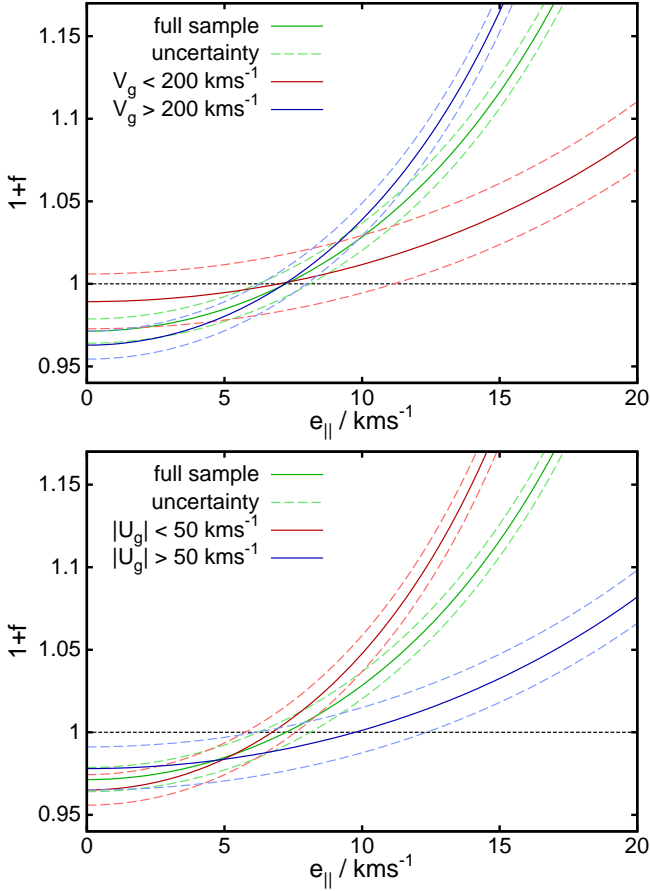


**Figure 10.** Both panels show the distance estimator  $1+f$  against the assumed  $v_{\text{los}}$  source dispersion  $e_{\parallel}$  for the LAMOST sample. In these plots,  $e_{\parallel}$  can be determined by demanding an unbiased distance estimator  $1+f \sim 1$ . The full sample is shown with green lines, dashed lines show the  $1\sigma$  error interval. The right combination of  $f$  and  $e_{\parallel}$  can be tested by cutting the sample into stars with a large vs. small baseline in  $VT_{VW}$  or  $UT_{UW}$  and demanding mutual agreement. In the top panel, we cut in galactocentric azimuthal velocity  $V_g$ , and in the bottom panel we cut in the radial velocity  $U_g$ . These subsamples are shown with red and blue lines in each panel.

### 5.5.1 Separating distance bias and line-of-sight velocity errors

Can we separate the line-of-sight velocity errors from a true distance error? In a larger sample, we can. The idea behind this is tested with the red and blue lines in Fig. 10. These lines show a separation of the LAMOST sample into subsamples with large and small  $V_g$  (top panel), or subsamples with large and small  $U_g$  (bottom panel). We recall that  $f$  is estimated based on the correlation of vertical velocities  $W$  with the baseline ( $y$ ) components  $T_{VW}V$  and  $T_{UW}U$ , measured by the covariance  $\text{Cov}(W, y)$  in equation (8). The selection in this plot target subsamples with a larger or smaller baseline  $y$ , i.e. while  $f$  is similar, both the covariance terms and the variance in the denominator of equation (8) vary. In contrast, the bias on the covariance from the  $v_{\text{los}}$  source dispersion is approximately the same, since it only depends on the sample geometry and  $e_{\parallel}^2$ . If the bias from  $e_{\parallel}$  dominates the distance statistics, we hence expect the different sample

selections in Fig. 10 to have the same  $1+f$  close to 1 at the correct value of  $e_{\parallel}$ , but the sample chosen to be closer to the Sun’s velocity (blue lines in Fig. 10) should have a steeper relationship of  $1+f$  against  $e_{\parallel}$  with larger curvature than its counterpart with larger heliocentric velocities (red lines). As a consequence, the low velocity selection (blue) should also have a larger deviation of  $1+f$  from 1 at  $e_{\parallel} = 0$ , exactly what is observed in Fig. 10. In contrast, if the measured deviation is a distance error,  $1+f$  of the subsamples should be in agreement at small values of  $e_{\parallel}$ . In Fig. 10 both ways to separate the sample agree perfectly on  $1+f \sim 1$  at an  $e_{\parallel} \sim 7 \text{ km s}^{-1}$ . However, we also note that the still moderate sample size limits the statistical significance: the discrimination on LAMOST without our prior knowledge from RAVE only barely excludes  $e_{\parallel} \sim 0$ .

The cut can be done either in  $V_g$  (top) or  $U_g$  (bottom panel), but it has to be done in galactocentric velocities, since a heliocentric selection would slice through the velocity ellipsoid at an angle and hence correlate  $W$  and the horizontal components. Another strategy would be to select the sample at different values of  $T_{VW}$  and  $T_{UW}$ , since the bias term has a quadratic dependence on these, or to use e.g. a metallicity cut to select kinematically hotter stars that have a larger baseline  $y$  by their larger velocities.

Each of these options has their caveats: The kinematic cuts in  $U_g$  or  $V_g$  select to some extent for the errors we are measuring. Stars with larger velocity errors (either from distance or from velocity uncertainties) are pushed towards the tails of the velocity distribution. A good position to cut in a larger sample are hence the points in the velocity distribution where it has a small or vanishing slope. If one selects in metallicity, the major caveats are a possible difference in the binary fraction, or also a correlation of  $\sigma_{\text{los}}$  with the metallicity (typically  $\sigma_{\text{los}}$  increases for metal-poor, hot stars).

### 5.6 Assessing the line-of-sight velocity uncertainty in RAVE

While the main measurement for the LAMOST sample is the line-of-sight velocity errors, the situation in the RAVE sample is far less clear. RAVE line-of-sight velocities have typically errors smaller than  $\sigma_{\text{los,RAVE}} \lesssim 2 \text{ km s}^{-1}$ , i.e. an order of magnitude smaller than the LAMOST uncertainties. Consequently, we get a precise measurement on LAMOST line-of-sight velocity errors, but we just see that something is wrong with the RAVE sample, either stellar distances being too short, or some contamination with larger  $v_{\text{los}}$  errors, or binary systems contaminating the data.

Fig. 11 gives an overview of the trade-off between parallax/distance bias and  $e_{\parallel}$ , similar to Fig. 10. From the earlier analysis we know that a major part of the problems can be ascribed to the suspected binary systems, so we show the full RAVE sample on the left-hand side and the suspected binary stars on the right-hand side. Note that the subsample of suspected binary stars with  $< 6000$  stars is very small, so the further separations (which have only 400 stars in the low- $V_g$  component) should be taken with caution due to small number statistics.

As we can see from the entire sample printed in green on the left-hand column, the full sample has a significant average distance underestimate ( $1+f < 1$ ) if we assume  $e_{\parallel} \lesssim 1 \text{ km s}^{-1}$  as suggested by the  $\sigma_{\text{los,RAVE}}$  estimates of the

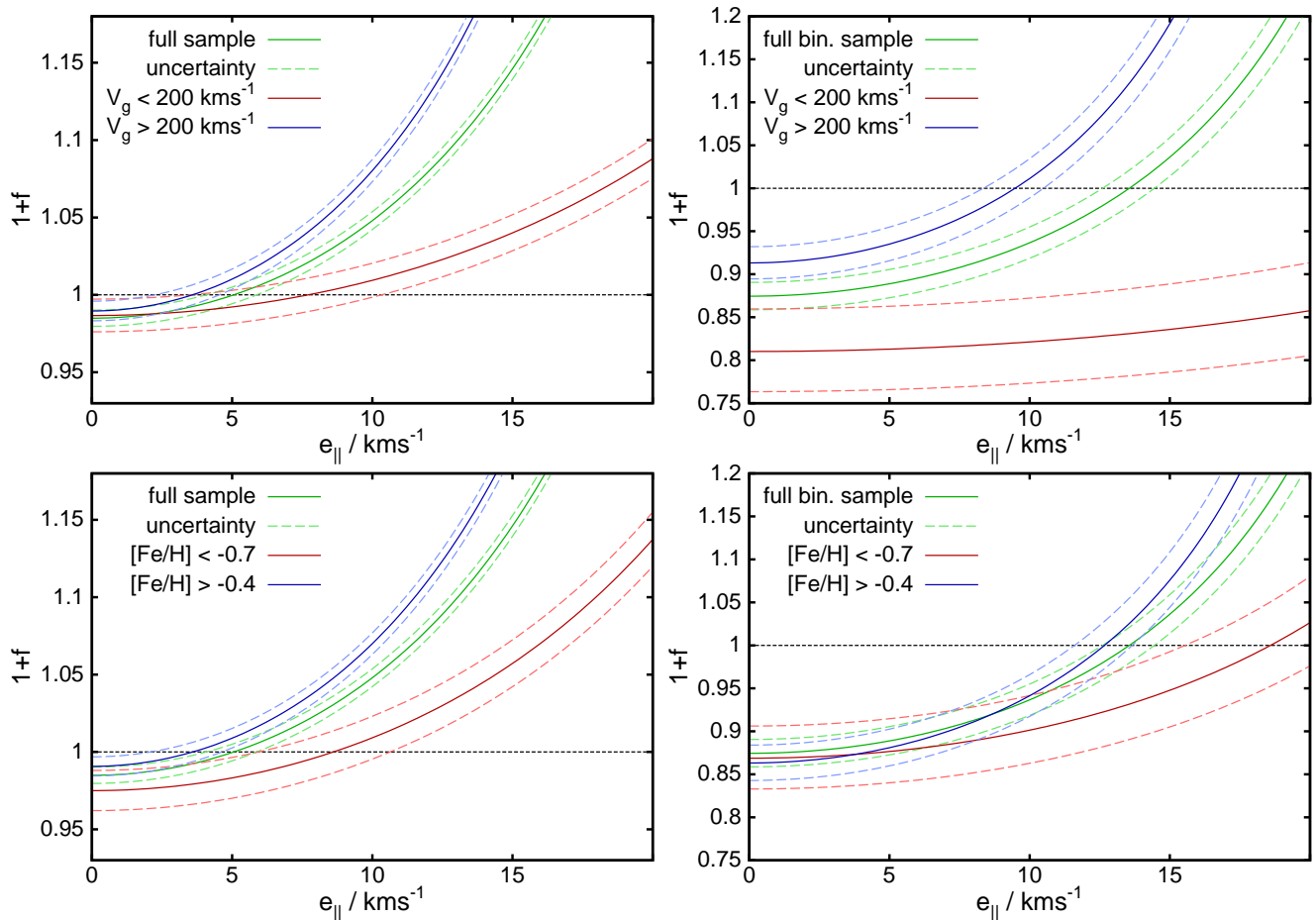


**Figure 11.** Distance bias  $1+f$  vs.  $v_{\text{los}}$  source dispersion  $e_{\parallel}$  in RAVE for the entire sample (left-hand column) and for the subsample carrying binary flags (right-hand column). The plots are organised as in Fig. 10, the green lines show the full sample, blue lines the subsample with smaller heliocentric velocities, and red lines the subsample with larger heliocentric velocities. Here the top panels show a separation at  $V_g = 200 \text{ km s}^{-1}$ , the bottom row shows a separation in metallicity, selecting once stars with  $[\text{Fe}/\text{H}] < -0.7$  dex and once with  $[\text{Fe}/\text{H}] > -0.4$  dex. The top right plot should be taken with some caution, since the low- $V_g$  binary sample only contains  $\sim 400$  stars.

RAVE pipeline, which tested fine in the statistics of Section 5.2. If we assumed that GAIA-TGAS and our distance derivation were completely bias-free, we would conclude that  $e_{\parallel} \sim 5 \text{ km s}^{-1}$ . It would be very unlikely that this is caused by large  $v_{\text{los}}$  measurement error in light of our findings in Section 5.2. Just like in LAMOST, we attempt to break the degeneracy by separating the sample in  $V_g$  (top panel) and in metallicity (bottom panel). This sample, however, is biased towards younger stars with small velocity dispersions and disc populations, so we have few useful halo stars. Both separations barely scratch statistical significance in the region of interest. Demanding agreement between the sub-samples, we can only conclude that  $e_{\parallel} < 5 \text{ km s}^{-1}$ , and that the statistics favour a problem with the stellar distances. We note that the values for  $e_{\parallel}$  are at least at the upper end of what might be achievable by binary systems (Hargreaves et al. 1996; Olszewski et al. 1996). We tested that a change of the parallax quality to  $\sigma_p/p < 10\%$  yields no significant difference.

The two panels on the right-hand side of Fig. 11 attempt the same dissection on the subsample of suspected binary stars. While assuming unbiased distances for this subsample would yield a  $v_{\text{los}}$  source dispersion  $e_{\parallel} \sim 14 \pm 2 \text{ km s}^{-1}$ , slicing

the sample into subsets of either low and high azimuthal velocity (top panel) or low and high metallicity (bottom panel) fails to convince that a velocity dispersion  $\sigma_{\text{bin}}$  caused by binary stars is the sole explanation. As discussed above, the samples with large intrinsic baselines in  $VT_{VW}$  and  $UT_{UW}$  (i.e. the low- $V_g$  sample, or the metal-poor subsample) should then start at a value of  $1+f$  closer to 1 at  $e_{\parallel} = 0$ , and intersect with their small-baseline counterpart at near-zero distance bias  $f$ . Here we observe the opposite. The low- $V_g$  subsamples (red lines) start already at more extreme  $1+f$  than the high- $V_g$  subsample (blue lines). There is no agreement between the subsamples anywhere near the region of  $1+f \sim 1$ . Both the top and the bottom panel suffer from the same discrepancy, though the bottom panel shows a milder version, while having different potential biases: the top panel possibly suffers from a potential direct kinematic bias, whereas the bottom panel could be impacted by binaries being wrongly evaluated as particularly metal-poor. This would be a reasonable suspicion in a low-resolution spectroscopic survey like RAVE. The unresolved binary broadens the lines, and while the equivalent width should not be strongly lowered, different line-shapes might have this effect. In addition the more metal-poor stars could have unaccounted  $v_{\text{los}}$  determi-

nation errors affecting both separations. A potential way out would be to claim that the Matijević et al. (2012) classification strongly depends on metallicity, but the most straightforward explanation is that TGAS astrometry fails for binary systems, in addition to some contribution by  $e_{\parallel}$ .

What we should take from this section is: Once we have a larger sample with certainly clean astrometry and a  $v_{\text{los}}$  determination at the quality level of RAVE and later Gaia, this method will be able to constrain even the binary velocity dispersion for different samples, and to differentiate well between  $e_{\parallel}$  and distance uncertainties. The sizes of the current samples are just at the boundary of offering a full solution which breaks the degeneracy. And, we can clearly see from these statistics that stars with binary flags should be excluded from any analysis.

## 6 CONCLUSIONS

In this work we have derived distance expectations and kinematics for stars in the RAVE-TGAS and LAMOST-TGAS samples.<sup>3</sup> We have applied the statistical methods developed by SBA to estimate the distance bias  $f$  in the RAVE-TGAS and the LAMOST-TGAS samples, and provide a set of validated stellar distances and kinematics. While there are several papers testing the accuracy and precision of parallaxes from Gaia-TGAS, even perfectly unbiased parallaxes do not guarantee unbiased distances, since there is a large uncertainty in estimating the right priors and selection functions, which enter a Bayesian distance estimate. Our method uses correlations of derived velocities with position in the sky, and hence directly tests the derived distances. We have validated this method using a realistic Galaxy simulation, for which we know the exact distances, as shown in the Appendix.

We find that the entire RAVE-TGAS sample shows statistically a global distance underestimate by of order 2–3%. However, more than half of this signal disappears when we restrict the sample to a subset of stars that are flagged as fully normal objects according to the classifications of Matijević et al. (2012), which detect binaries or peculiar stars, e.g. with emission lines. We have demonstrated that the objects with at least one binary flag show distance statistics equivalent to distance underestimates in excess of 15%.

While it would be tempting to put all the blame of the distance bias on TGAS parallaxes, we have shown that distance statistics  $f$  are biased proportional to the source  $v_{\text{los}}$  variance  $e_{\parallel}^2$ . This comprises  $v_{\text{los}}$  measurement errors and contamination with binary stars, which act like a distance underestimate on  $f$ . On the one hand this requires that we find a way to differentiate  $e_{\parallel}$  from a true distance bias. On the other hand it is a useful way to measure  $e_{\parallel}$  and hence determine  $\sigma_{\text{los}}$  on samples where parallaxes are good and the  $e_{\parallel}$  dominates the  $f$  estimates. We can use this dependence of  $f$  on  $e_{\parallel}$  in two ways: i) we can vary  $e_{\parallel}$  with the condition  $f \sim 0$ , and thus measure  $e_{\parallel}$ ; ii) we can probe the accuracy

of  $\sigma_{\text{los}}$  estimates in a pipeline by separating each sample in  $\sigma_{\text{los}}$  and looking for trends in  $f$ .

The LAMOST sample demonstrates this capability. Our method has revealed that the uncertainties given by the LAMOST pipeline have no detectable information content for uncertainties below  $\sigma_{\text{los,LAM}} < 27 \text{ km s}^{-1}$ , while stars with larger  $\sigma_{\text{los,LAM}}$  show a sudden increase in  $e_{\parallel}$ . More importantly, when comparing the full distance estimator  $f$  with its counterpart  $f_V$  that uses only the azimuthal  $V$  velocity vs. the vertical motion  $W$ , these two estimators yield highly inconsistent results. We also find that the LAMOST sample shows a near-perfect relationship between  $W$  and  $\sin(b)$ , indicating a  $5 \text{ km s}^{-1}$  offset in the  $v_{\text{los}}$  measurements, while RAVE has no significant correlation. When we correct LAMOST for this  $\delta v_{\text{los}} = 5 \text{ km s}^{-1}$ , we measure  $e_{\parallel} = 7.2 \pm 1 \text{ km s}^{-1}$  with a systematic uncertainty of about  $2 \text{ km s}^{-1}$ , i.e. the LAMOST  $v_{\text{los}}$  measurements are far more precise than indicated by their nominal errors.

In RAVE, the full sample starts showing signs of increased  $e_{\parallel}$  above  $\sigma_{\text{los,RAVE}} \geq 1.5 \text{ km s}^{-1}$ , and these reach an unacceptable level above  $5 \text{ km s}^{-1}$ . This behaviour is not detectable when we restrict the sample to unflagged/normal stars, i.e. the flags indicate the most problematic  $v_{\text{los}}$  determinations.

We have demonstrated how to measure the selection function  $S(s)$  and distance prior of each sample from the data directly in Section 5.3.1. We start from a flat  $S_0(s)$ , measure a new  $S_1(s)$  by comparing the stellar distance distribution to the expectation in the prior, and then iteratively insert this selection function into the distance determinations. This procedure converges within 5 iterations. By separating the sample in distance, we can show that neglect of this selection function (i.e. a flat  $S(s)$ ) results in catastrophic distance bias towards larger distances, while the derived selection function provides unbiased distances within the measurement accuracy.

It is generally inadvisable to use the naive parallax estimator  $s' = 1/p$  for stellar distances, because it neglects the proper transformation of the parallax error distribution into  $s$ , which gives a large distance underestimate against the true expectation value  $\langle s \rangle$ . However, to our surprise, we find that on both RAVE and LAMOST-TGAS this estimator results only in a mild distance underestimate. The reason for this is that the selection function/distance prior falls steeply towards larger  $s$ , compensating partly for the missing transformation.

We note that the distance estimator  $f$  for RAVE stars with very short distances ( $\langle s \rangle \lesssim 0.15 \text{ kpc}$ ) consistently indicate distance underestimates. This can either be an extreme statistical fluctuation, or it might indicate either a problem with the largest TGAS parallaxes, or a stronger selection against stars with large proper motions than indicated in Lindegren et al. (2016).

We have detected an anomaly either in the stellar kinematics or in the parallaxes for the RAVE-TGAS sample around a galactic longitude  $l \sim 300^\circ$ , and at a distance of  $0.3 < s/\text{kpc} < 0.35$ . The feature is found on both sides of the Galactic plane, and the correlation between vertical and azimuthal velocities is neither found in its foreground nor in its background. The same sign on both sides of the plane argues strongly against a (halo) stellar stream as source of

<sup>3</sup> Please find the datasets with distances and kinematics and our source code at <http://www.thphys.physics.ox.ac.uk/people/RalphSchoenrich/data/tgas-dist/data.tar.gz>, or request them directly from the authors.

this. The feature is also robust against outliers, and cannot be explained by eventual anomalies in the selection function. A likely explanation is substructure at this position in the Galaxy, e.g. a breathing mode near a spiral arm or spur, though we are not aware of such a feature at this position. Further analysis will be required to understand if this is a possible localised failure of TGAS astrometry, or in the other case, to unravel the exact nature of this structure.

We have further shown that the degeneracy between  $v_{\text{los}}$  source dispersion  $e_{\parallel}$  and a true distance bias can be broken by selecting subsamples with different lengths of baseline in  $VT_{\text{VW}}$  or  $UT_{\text{UW}}$ . This is achieved by splitting the sample either with a metallicity selection or directly in stellar kinematics. The larger upcoming Gaia data releases will be sufficient to make this method work. In the current samples, this ability is just borderline significant. It shows that while we have a consistent picture for LAMOST being dominated by line-of-sight velocity uncertainties, the statistics suggest that the deviations in the RAVE survey, in particular on the binary subsample, derive from a combination of astrometric problems and intrinsic  $v_{\text{los}}$  dispersion.

## ACKNOWLEDGEMENTS

It is a pleasure to thank Laurent Eyer, James Binney, and Paul McMillan for helpful discussions and comments. This work used the DiRAC Data Centric system at Durham University, operated by the Institute for Computational Cosmology on behalf of the STFC DiRAC HPC Facility ([www.dirac.ac.uk](http://www.dirac.ac.uk)). This equipment was funded by a BIS National E-infrastructure capital grant ST/K00042X/1, STFC capital grant ST/K00087X/1, DiRAC Operations grant ST/K003267/1 and Durham University. DiRAC is part of the National E-Infrastructure. This work was supported by the European Research Council under the European Union's Seventh Framework Programme (FP7/2007-2013)/ERC grant agreement no. 321067.

## REFERENCES

- Arenou F. et al., 2017, arXiv:1701.00292  
Aumer M., Binney J., Schönrich R., 2016, MNRAS, 459, 3326  
Aumer M., Binney J., 2017, submitted  
Astraatmadja T., Bailer-Jones C., 2016, ApJ, 832, 137  
Binney J. et al., 2014, MNRAS, 439, 1231  
Burke B.F., 1957, AJ, 62, 90  
Davies G.R. et al., 2017, arXiv:1701.02506  
De Ridder J., Molenberghs G., Eyer L., Aerts C., 2016, arxiv:1609.08945  
Debattista V., 2014, MNRAS, 443, 1  
Dehnen W., 1998, AJ, 115, 2384  
Dehnen W., 2000, AJ, 119, 800  
Djorgovski S., Sosin C., 1989, ApJ, 341, 13  
Faure C., Siebert A., Famaey B., 2014, MNRAS, 440, 2564  
Gaia Collaboration et al., 2016, A&A, 595, 2  
Gieles M., Sana H., Portegies Zwart S., 2010, MNRAS, 402, 1750  
Girardi L., Salaris M., 2001, MNRAS, 323, 109  
Hargreaves J.C., Gilmore G., Annan J.D., 1996, MNRAS, 279, 108  
Høg E. et al., 2000, A&A, 355, 27  
Ivezic Z. et al., 2008, ApJ, 684, 287  
Kepley A. et al., 2007, AJ, 134, 1579

- Kerr F.J., AJ, 62, 93  
Kunder A. et al., 2016, arXiv:1609.03210  
Lindegren et al., 2016, A&A, 595, 4  
Liu X.-W., Zhao G., Hou J.-L., 2015, RAA, 15, 1089  
Luo A.-Li et al., 2015, RAA, 15, 1095  
McMillan P., 2011, MNRAS, 414, 2446  
Matijević G. et al., 2012, ApJS, 200, 14  
Olszewski E., Pryor C., Armandroff T., 1996, AJ, 111, 750  
Pérez-Villegas A., Portail M., Wegg C., Gerhard O., 2017, arXiv:1702.06541  
Perryman M., 1997, A&A, 323, 49  
Perryman M., 2001, A&A, 369, 339  
Reid M.J. et al., 2014, ApJ, 783, 130  
Salaris M., Girardi L., 2002, MNRAS, 337, 332  
Schönrich R., Binney J., Dehnen W., 2010, MNRAS, 403, 1829  
Schönrich R., 2012, MNRAS, 427, 274  
Schönrich R., Binney J., Asplund M., 2012, MNRAS, 420, 1281  
Schönrich R., Bergemann M., 2014, MNRAS, 443, 698  
Siebert A. et al., MNRAS, 2008, 391, 793  
Steinmetz M. et al., 2006, AJ, 132, 1645  
Strömberg G., 1927, ApJ, 65, 238  
van Leeuwen F., 2007, ASSL, 350, 1  
Vogt S., Mateo M., Olszewski E., Keane M., 1995, AJ, 109, 151  
Wang S., Su D., Chu Y., Cui X., Wang Y., 1996, ApOpt, 35, 5155  
Wojno J. et al., 2016, arXiv:1611.00733v1  
Xu Y., Newberg H.J., Carlin J.L., Liu C., Deng L., Li J., Schönrich R., Yanny B., 2015, ApJ, 801, 105

## APPENDIX A: VALIDATION ON GALAXY SIMULATIONS

To perform a sanity check on our method and to confirm its robustness against galactic substructure, we employ galaxy simulations that resemble the Milky Way. The simulations are described in detail in [Aumer et al. \(2016\)](#) and [Aumer & Binney \(2017\)](#). They feature a reasonable bar, have appropriate thin and thick disc components and an active spiral pattern.

We focus on model  $V\alpha 9s8\lambda\zeta$ . To build this model, we continuously add stellar particles on disc orbits to a model galaxy within a live dark matter halo over the course of 12 Gyr. The birth velocity dispersions of the stellar populations decline continuously in this model, from  $> 40 \text{ km s}^{-1}$  during the first 1.5 Gyr to essentially near-circular orbits after 4 Gyr. This creates a disc galaxy with reasonable thin and thick disc components.

Moreover, the model grows inside-out with a declining star formation history.  $V\alpha 9s8\lambda\zeta$  has a final baryonic mass  $M_{\text{baryons}} = 6 \times 10^{10} M_{\odot}$ , and a live dark matter halo with mass  $M_{\text{dm}} = 1 \times 10^{12} M_{\odot}$ , which is set up with an initial concentration parameter of  $c = 6.5$ .

At our evaluation time 12 Gyr, the vertical profile is double-exponential. At  $R = 8 \text{ kpc}$ , it can be fitted with exponential scaleheights  $h_{z,\text{thin}} \approx 285 \text{ pc}$  and  $h_{z,\text{thick}} \approx 990 \text{ pc}$ . The thick disc contributes  $\sim 20\%$  to the local surface density. The final model has a bar of length  $\sim 4 \text{ kpc}$ . Its  $R = 8 \text{ kpc}$  circular speed, dark matter density and baryonic surface density compare reasonably with observational constraints for the Solar neighbourhood. The level of radial migration in the model agrees with constraints from MW chemical evolution and its Solar neighbourhood velocity distributions show good agreement with RAVE+TGAS data if one corrects for

**Table A1.** Distance error estimates  $f$  in simulations with perfect distances. Each simulation has 25 samples around  $R = 8$  kpc at equidistantly spaced positions in azimuth. The first three columns give statistics for the full distance estimator  $f$ .  $\langle f \rangle$  is the mean value of  $f$  from averaging over all 25 samples,  $\sigma_f$  is the residual dispersion of  $f$ , and  $\sigma_{f,st}$  is the average of the statistical errors derived with  $f$ . If the estimates are true, then  $\sigma_f$  should be close to  $\sigma_{f,st}$ . Systematic biases in  $f$  depending on the sample position would show as  $\sigma_f$  significantly larger than  $\sigma_{f,st}$ . The last three columns give the same statistics for  $f_V$ .

model	$\langle f \rangle$	$\sigma_f$	$\sigma_{f,st}$	$f_V$	$\sigma_{f,V}$	$\sigma_{f,V,st}$
V $\alpha$ 9s8 $\lambda\zeta$	0.0007	0.015	0.014	0.0022	0.033	0.022
V $\alpha$ 5 $\lambda$	-0.0087	0.019	0.013	-0.0072	0.024	0.019
M $\alpha$ 1 $\zeta^*$	0.0030	0.019	0.017	-0.0001	0.030	0.027
P2	-0.0067	0.020	0.017	-0.0085	0.035	0.028
EHR2	-0.0079	0.011	0.008	0.0019	0.015	0.013

selection effects. Overall, the model is well suited to create mock Solar neighbourhood samples.

To create these samples, we place the observer at  $(R, z) = (8.3, 0)$  kpc choosing 25 different positions, which are equally distributed in galactocentric azimuth  $\Phi_{gal}$ . We then select all stars with distances  $s < 1$  kpc, obtaining samples of about 15 – 20000 stars each. In these samples, we calculate the stellar positions, proper motions and line-of-sight velocities using a solar motion of  $(U_\odot, V_\odot, W_\odot) = (11, 250, 7)$  km s $^{-1}$  (we note that the only effect of the set solar motion is to alter the length of the baseline component  $T_{VW}V$  and thus the precision of  $f$ ). Fig. A1 shows the tests of our distance statistics on these quite realistic samples. The top panel shows the full distance estimator  $1+f$  for each of the 25 observer positions in  $\Phi_{gal}$ . The test statistics are consistent with a perfectly unbiased estimator. There are 9 datapoints beyond  $1\sigma$ , which is just the expected number of outliers.

The mean distance estimator  $\langle f \rangle$  in each sample, the dispersion of the distance estimates  $\sigma_f$ , and the expected dispersion from shot noise and uncertainty in the correction of the velocity ellipsoid tilt  $\sigma_{f,st}$  for model V $\alpha$ 9s8 $\lambda\zeta$  are summarized in the first line of Table A1. We also show the numbers for four additional Milky Way like models. Models V $\alpha$ 5 $\lambda$  and M $\alpha$ 1 $\zeta^*$  are of the same type as V $\alpha$ 9s8 $\lambda\zeta$ , but differ in model parameters and consequently in structural details at final time. Models P2 and EHR2 also contain both thin and thick disc components, but the thick disc components are created as initial conditions and the thin disc is populated with stars born on near-circular orbits over 10 Gyr.

The values for all five models included in Table A1 demonstrate that, on average, the distance statistics show no bias at the levels needed for this work (generally less than 1%). Moreover, the statistically expected scatter almost matches the observed scatter in  $1+f$ , i.e. any impact by unaccounted systematics in the samples is significantly below 1%. We note that the dispersion values are lowest in EHR2 as this model has a higher resolution than the other four.  $f_V$  is in principle more vulnerable to disc structure, but we see no clear indication for a significant additional scatter in its statistics provided in the three right-hand columns.

As detailed in Section 4.3 the fits become more risky when we separate samples in longitude and/or latitude, because effects caused by galactic structure do not cancel out any more to first order. This is particularly the case for simulation EHR2, which has a longer bar than the Milky Way.

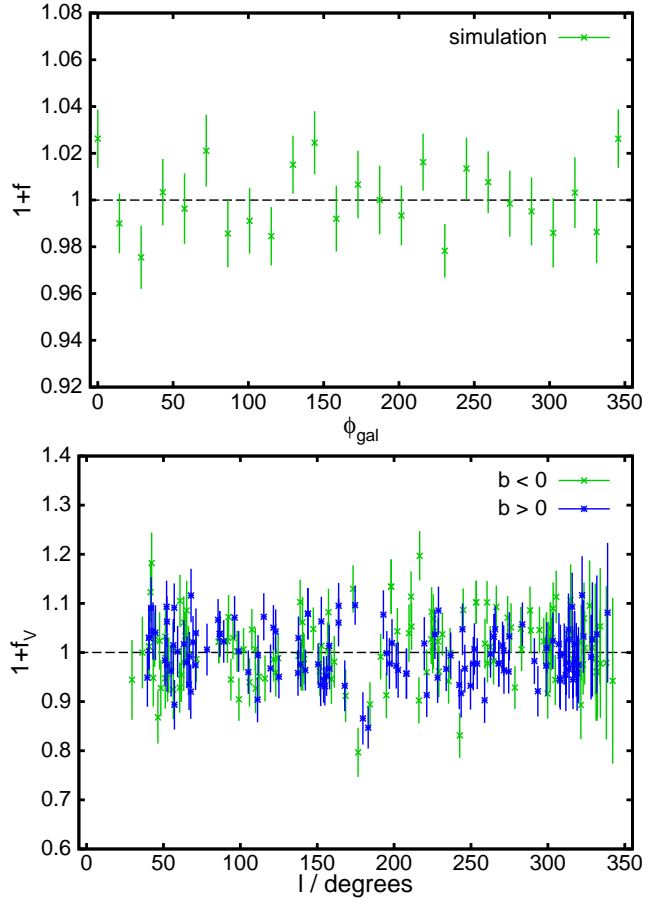


**Figure A1.** Testing the distance estimator on N-body galaxy model V $\alpha$ 9s8 $\lambda\zeta$ . The top panel shows the distance statistics for 1 kpc sized samples taken around simulated solar positions at  $(R, z) = (8.3, 0)$  kpc, equally spaced in azimuth  $\Phi_{gal}$  (x-axis). The bottom panel shows the restricted distance estimator  $f_V$  when we bin each sample in Galactic longitude  $l$  (x-axis) and separate the sample into positive (blue) and negative (green) galactic latitude  $b$ .

As the bar thus has a larger impact at  $R = 8$  kpc, in that simulation, cutting the test samples at  $l = 180^\circ$  results in a scatter of  $\sim 5\%$  in  $f_V$ . As expected, most of this gets compensated in the full estimator  $f$ , which has just 2% dispersion (compared to about 1.2% statistically expected dispersion). This simulation shows a discernible  $m = 2$  pattern when the  $f_V$  statistics are plotted against  $\Phi_{gal}$ .

The bottom panel in Fig. A1 looks for trends in the restricted distance estimator  $f_V$  when separating simulation V $\alpha$ 9s8 $\lambda\zeta$  from the top panel in galactic longitude  $l$ , selecting subsamples of 3000 stars each. Before ordering the sample in  $l$  we have additionally cut it into northern and southern hemisphere ( $b > 0$  and  $b < 0$ ). There is no detectable systematic deviation, apart from a minor issue with the error determination near  $l = 180^\circ$ . At that position  $T_{VW} \sim 0$ , i.e. there is virtually no signal for  $f_V$ , which also affects the error determinations in a small region.

Similarly, the increase in uncertainties of  $f_V$  is due to the vanishing of  $T_{VW}$ . Overall, the statistics of this sample look fine - due to the cold stellar kinematics, and the small sample sizes, the statistically expected errors are  $\sim 12\%$ , close to the observed dispersion.